공학박사학위논문

Dynamic Characteristics of Open and Closed type Swirl Injectors with Varying Geometry

Open-type과 Closed-type 스월 인젝터의 형상변화에 따른 동특성 연구

2017년 2월

서울대학교 대학원
기계항공공학부
정연재

ABSTRACT

Injector is one of the key component in liquid rocket engines especially when suppressing the combustion instability. Since the injector is located between the feed line and the combustor, injector plays a role as the bridge between the two components. The stable combustion can be achieved if the injector is desgined to be dynamically robust to suppress the feedback interactions among the three components. Therefore, dynamic characteristics of the injector should be investigated in order to establish criteria for injector modification. Open-type and closed-type swirl injectors have been widely used in liquid rocket engines. The type of the swirl injector should be selected based on its pros and cons. However, comparisons between the dynamic characteristics of the open and closed type swirl injectors are not thoroughly studied and further research should be done. In this study, dynamic characteristics of the each open and closed type swirl injectors with varying geometries were investigated through experiments. Influences of diameter of the manifold, diameter of the swirl chamber, length of the swirl chamber, converging angle between the swirl chamber and orifice, and length of the orifice were analyzed.

Sinusoidal pressure fluctuations were generated by the hydrodynamic mechanical pulsator to simulate the external disturbances in the actual operation of liquid rocket engine. The feed line pressure measured with static and dynamic pressure sensors were selected as the input parameter and the liquid filim thickness at the injector exit measured with the titanium electrodes were selected as the output parameter since it is closely related with the mass flow rate of the swirl injector. Transfer function between the input and output parameters were obtained throughout the pulsation frequencies of 100 – 1000 Hz. The dominant geometry parameter for each open and closed type swirl injectors were verified.

With the obtained experimental data of each geometry parameters sensitivity and tendency, directions for injector design modifications can be given when the combustion instability occurs during the development of a liquid rocket engine.

Keywords: open type swirl injector, closed type swirl injector, feed line, swirl chamber, orifice, hydrodynamic mechanical pulsator, dynamic characteristics, liquid film thickness, mass flow rate,amplitude, phase.

Student Number: 2010-30967

LIST

LIST OF FIGURES

LIST OF TABLES

NOMENCLATURE

P_f	pressure in the feed line, bar
P_m	pressure in the manifold, bar
P_o	pressure in the orifice, bar
P_e	pressure at the exit of the swirl chamber, bar
D_m	manifold diameter, mm
D_s	swirl chamber diameter, mm
L_s	swirl chamber length, mm
L_e	extended swirl chamber length, mm
t_o	liquid film thickness at the end of the orifice, μm
t_e	liquid film thickness at the exit of the swirl chamber, μm
α_c	converging angle, degree
θ	spray cone half angle, degree
n_t	tangential entry number
$\Pi_{\text{т}}$	tangential entry transfer function
$\Pi_{\text{к.зII}}$	swirl chamber transfer function by surface wave
$\Pi_{\text{к.зIII}}$	swirl chamber transfer function by vorticity wave
$\Pi_{\text{к.сII}}$	orifice transfer function
φ	filling coefficient
$Sh_{\text{т}}$	strouhal number in tangential entry
A	injector geometry coefficient

Subscripts

f	feed line
m	manifold
o	orifice
e	exit of swirl chamber
t	tangential entry

s	swirl chamber
c	converging section
avg	averaged term

Superscripts

‾	normalized term
′	fluctuated term

CHAPTER 1

INTRODUCTION

From the very first day the human race has set foot in the space, liquid rocket engine has been the primary mean to deliver payload on the orbit. Despite new technologies and materials have been developed over the decades, liquid rocket engine is still being used and improved. In the process of liquid rocket engine development, one of the most important issue is combustion instability in the combustion chamber.

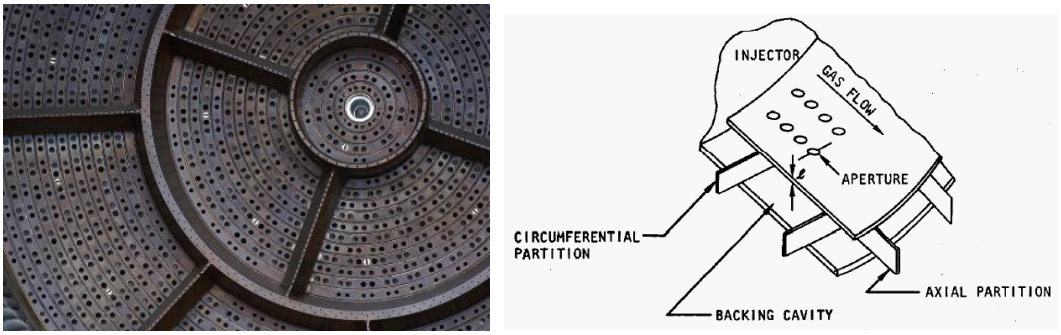

Fig. 1.1 Baffle and acoustic cavity (ref. [1]).

The typical approaches of combustion instability suppression are baffle and acoustic cavity which are illustrated in Fig. 1.1. Generally, combustion instability results from a coupling of the combustion process and the fluid dynamics of the engine. Therefore, combustion instability can be suppressed by reducing the coupling of the oscillations and the driving combustion process or by increasing the damping inherent in the engine system. The device to reduce coupling is the combustion chamber baffles and the device to increase damping is the acoustic cavities. However, these well-known solutions need additional structures in the combustion chamber which spoil the efficiency of the liquid rocket engine and increase the mass of the liquid rocket.[1] Regardless, in Russia, where swirl-type injectors are widely used, means to suppress combustion

instability by modifying the injectors were incorporated. By treating the problem with this alternative approach, they were able to remove the instability without additional structures. The study of this method is called injector dynamics.[2, 3] Injector dynamics is a study that focuses on the dynamic responses of the injector to dynamic disturbances.

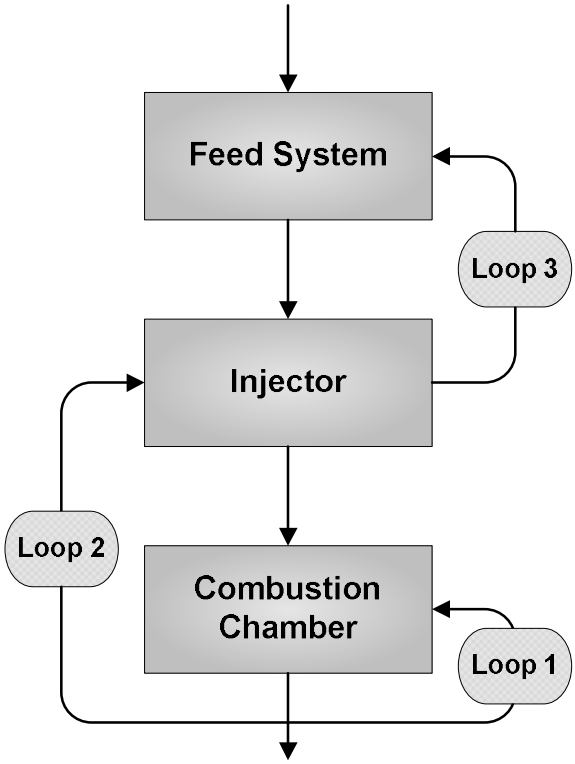

Fig. 1.2 Schematic of dynamic interactions in the rocket engine system (ref. [4]).

Figure 1.2 shows the schematic of dynamic interactions among the three major elements of the liquid rocket engine system, which are the feed system, the injector, and the combustion chamber. In the operation of the liquid rocket engines, the propellants are supplied to the injector through the feed system, and they experience atomization, vaporization, and mixing process when injected into the combustion chamber by the injector. During the combustion process in the combustion chamber, a pressure oscillation

is generated, which affects the impending combustion process.(Loop1) Furthermore, that acoustic pressure oscillation will cause fluctuations in the injector's properties, such as the propellant velocity, pressure in the orifice, or mass flow rate.(Loop2) Finally, the oscillation in the injector can again excite the pressure in the feed system, which means the input parameters entering the injector will be more unstable, starting a negative feedback loop over the whole liquid rocket engine system if not properly controlled.(Loop3)[3, 5] These dynamic interaction loops were found in actual liquid rocket engine developments and properly suppressed through many experiments.[6] In the interactions among the three major elements of the liquid rocket engine system, the injector is located between the feed system and the combustion chamber, playing the role of a bridge that connects them. If the injector is properly designed, it can suppress the combustion instability by cutting changing the dynamic interaction loops. This mechanism is the motivation for injector dynamics studies.[2, 3] Recently, the importance of injector dynamics has been acknowledged worldwide, and several research groups are working on the topic. From the same origination—Bazarov's work—each group started to focus on different aspects of the injector's dynamic characteristics and the types of injectors. Though progress was made through the efforts of the research groups globally, many problems in injector dynamics studies remain unsolved.[5, 7-14]

To conduct the injector dynamics experiments, artificial pressure fluctuations in the feed line should be generated to simulate disturbances in the actual liquid rocket engine during its operation. Therefore, for the experiment, a hydrodynamic mechanical pulsator was designed and manufactured to generate sinusoidal input pressure oscillation in the feed line. Typically, in injector dynamics studies, the mass flow rate through the injector is taken as the output parameter. In this study, however, the mass flow rate through the injector was found to be inappropriate as the output parameter, and the liquid film thickness in the injector orifice was chosen instead. The reason for this selection will be discussed later in the paper. Prior to open-type swirl injectors, studies on closed-type swirl injectors were conducted.[3, 5, 8-10, 12, 14] Interest in research on the open-type swirl has increased relatively recently.[4, 15-17] As there has not been a long history of

research on open-type swirl injectors, a number of problems remain unsolved.

To apply the research results of injector dynamics studies to injector design, analyzing the amplitude of the output parameter in the frequency domain is the most important task. Therefore, experiments to measure the amplitude of the output parameter of simplex swirl injectors were conducted. Variations in the liquid film thickness amplitude with varying injector geometries were analyzed. Dominant geometry parameters for each type of swirl injector were investigated to verify their tendencies and sensitivities on the dynamic characteristics of the injector. Spray characteristics were investigated with visualization results to confirm that the internal characteristics appeared in the liquid film thickness results are observed in the external characteristics. From the dynamic characteristics data which were acquired through the experiment, physical mechanisms for the injector's behaviors were analyzed. The main objective of the study to find the dominant geometrical parameter and its tendency were achieved.

CHAPTER 2

EXPERIMENT AND MEASUREMENT SYSTEMS

2.1 Types of swirl injector

Liquid swirl injectors are widely used for their good atomizing performance and margin in manufacturing tolerance. Conventional swirl injector is composed of tangential entry, swirl chamber and orifice. The liquid enters the swirl chamber with circumferential velocity given by the tangential entry. The swirling motion of the propellant is stabilized in the swirl chamber and converging section between the swirl chamber and orifice accelerates the circumferential velocity by conservation of angular momentum. Finally, the propellant is discharged through orifice forming a conical sheet. Typical swirl injector can be divided into two types: closed and open-type swirl injector.

Figure 2.1 shows the schematics of each type of the swirl injector. The closed-type swirl injector includes a converging section between the swirl chamber and orifice to accelerates the circumferential velocity of the propellant. On the contrary, the open-type swirl injector has a straight swirl chamber which makes it much simple in design. The atomization quality of static spray sheet is better in closed-type swirl injector since the discharging velocity is higher due to the acceleration in converging section. The high discharging velocity makes the liquid film thickness thinner which means fine atomization. On the other hand, an open-type swirl injector has a constant swirl chamber radius which makes the liquid film thickness at the end of the injector thicker than that of a closed-type swirl injector, resulting in a relatively poorer atomization performance. Therefore, closed-type swirl injector is adopted usually in smaller engines where each injector's atomization performance is important. Large number of injectors are placed in large liquid rocket engine for high mass flow rate and their spray sheets interact with one another, this circumstance makes it less important for each injector's to have high

atomizing performance. For this reason, the open-type swirl injectors are adopted mostly in large liquid rocket engine systems. While these characteristics are confined to the static state, the dynamic characteristics of each injector have been investigated very little. In this research, the dynamic characteristics of closed and open-type swirl injectors with varying geometry conditions are investigated.

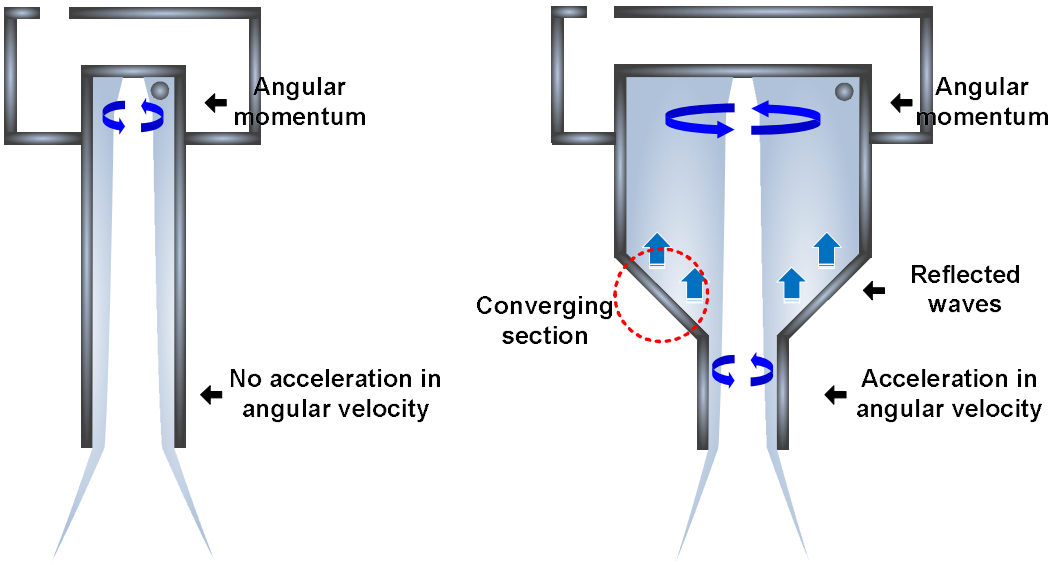

Fig. 2.1 Schematics of (a) open and (b) closed type swirl injector (ref. [4]).

2.2 Hydrodynamic mechanical pulsator

During the operation of liquid rocket engine, instabilities are generated from different sources over wide range of frequencies. Efforts to verify the mechanisms of the instabilities were given in the development of liquid rocket engines. Research has suggested identification of mechanisms and methods to control or eliminate the instability. However, there are part of the instabilities which remains unclear and needs more efforts to identify the mechanism and solution. The typical classification of instabilities which are inherent in liquid rocket engines are given in Table 2.1. They are divided into 3 types based on its frequency and mechanism.[18]

Table 2.1 Types of combustion instability in liquid rocket engine (ref. [19]).

Type	Name	Frequency
Low frequency combustion instability	Chugging	10 ~ 400
Mid frequency combustion instability	Buzzing	400 ~ 1000
High frequency combustion instability	Screeching	1000 ~

1. Low frequency, chugging. – Among the 3 types of instabilities in liquid rocket engines, chugging is known to be the easiest one to handle both from an analytical and experimental or developmental standpoint. This is a low frequency oscillation at a few Hertz in chamber pressure usually caused by pressure variations in feed lines due to variations in acceleration of the vehicle. This can cause cyclic variation in thrust, and the effects can vary from merely annoying to actually damaging the payload or vehicle. Methods to eliminate the

chug instability include increasing the pressure drop in the injector and increasing the fluid inertance by using gas-filled damping tubes on feed lines of high density propellants.

2. Mid frequency, buzzing. – This can be caused due to insufficient pressure drop across the injectors. It generally is mostly annoying, rather than being damaging. They may degrade performance, total impulse or thrust vector. However, in extreme cases combustion can end up being forced backwards through the injectors causing explosions with monopropellants or increase in amplitude to trigger a high frequency mode. Buzzing is often encountered in development programs on engines which are designed to throttle over a wide thrust range. Because the combustion is given a continuously varying set of conditions, it is nearly certain that at least one condition will be found to be favorable for coupling with wave motion in the propellant feed system.

3. High frequency, Screeching. – Instability in high frequency is the most destructive type and most difficult case to eliminate. The Screeching is generated by the coupling of acoustic pressure modes in the combustion chamber with heat release oscillation. Usually in corresponds with the calculated acoustic resonance frequencies of the combustion chamber. In large liquid rocket engines, the transverse and radial modes are found to be more destructive than the longitudinal modes. Elimination of high frequency instability is achieved in two typical ways. The first is to change the injector geometry to make changes in the propellant spray and combustion characteristics. Second is to increase damping of the liquid rocket engine system by adopting additional structures as baffles and acoustic cavities.

Despite the classifications and solutions listed above, it is not simple to distinguish the instabilities that appears in the operation of actual liquid rocket engines. Furthermore, the instabilities appear in combinations for various cases. For this reason,

the research on the dynamic characteristics of injectors should be in wide range of frequency to include various types of instabilities. And the first step to do so is to design and manufacture a robust device that generates a strong and fine periodical pulsation with wide range of frequency in the feeding line. With the device, injector's dynamic responses to the disturbances from low frequency to high frequency can be experimentally investigated. Table 2.2 shows the lists of such devices classified by its mechanisms.[20]

1. Hydraulic pulsator – Periodical fluctuation in the pressure of liquid or gaseous flow can be achieved by periodically exposing the test fluid to a decreased pressure source. Hydraulic method to obtain the periodic exposure is installation of rotating valve. The rotating valve does not impart any inertial force on the fluid and variation of the flow area can reach up to very high frequencies. A portion of the test fluid is wasted since it is diverted to generate oscillations.

2. Acoustic pulsator – Acoustic pulsators operate by excitation of pressure and velocity waves in the fluids which can be generated by a membrane, by a piston, or by means of piezo-electric or magnetostriction actuators. Pros and cons of acoustic pulsators are very clear. The quality of the generated harmonic oscillation is very fine so that it is preferred in small-scale physical experiments. However, the amplitude of the pulsation is rather weak compared to the other pulsator mechanisms.

3. Inertial pulsator – Inertial pulsator excites the oscillation by mechanically vibrating the part of the feed line. This type of pulsator has a simple design and is not exposed to leakage. The amplitude of the pulsator will be defined by the periodic displacement of mass of fluid. However, the cost of the system can be rather expensive since high power drive is required. Inertial type pulsators are well suited for high pressure condition of toxic or cryogenic fluids.

Table 2.2 Drive advantages and disadvantages (ref. [20]).

Types of drive	Advantages	Disadvantages
Hydrodynamic	• Low power requirements • High amplitude is possible • High frequency is possible • Strong pulsation in compressible fluids • Smooth and continuous • frequency control • Low noise during operation	• Non-harmonic pulsation • Wasted model liquid • Possible leakages • High friction parts • High speed rotation • Impossible with cryogenic, toxic and hypergolic liquids
Acoustic	• Harmonic oscillations • Possible with any liquid	• Weak pulsation amplitude • Frequency fixed by actuator • High power drive • High noise • Primarily for small scale experiments
Inertial	• No leaks • No friction • Wide frequency range • Possible with any liquid	• High power drive • High noise
Self oscillating	• Absence of external drive • Possible with any liquid • Possible with gases	• Dependence of frequency, amplitude and even the presence of pulsation on operational parameters of the studied flow

Fig. 2.2 Hydrodynamic mechanical pulsator.

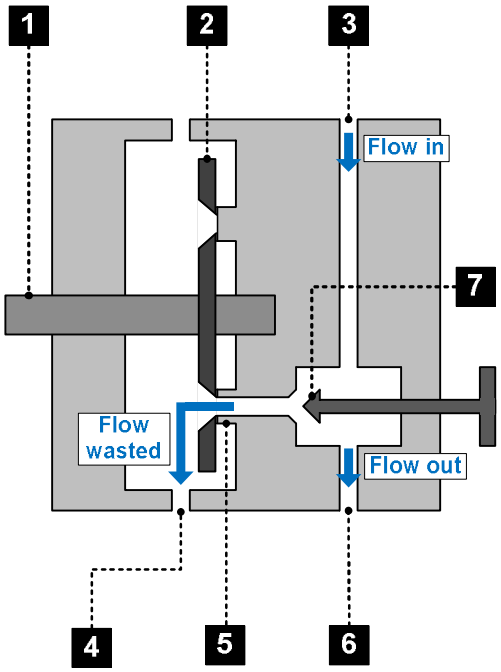

Fig. 2.3 Hydrodynamic mechanical pulsator: 1) shaft; 2) disk; 3) inlet port; 4) waste port; 5) connector; 6) outlet port; 7) throttle valve

The pulsator manufactured and used for the experiment is shown in Fig. 2.2. The type of the pulsator selected for current study is hydrodynamic mechanical pulsator which generates pressure oscillation with rotating disk driven by electrical motor with inverter. Figure 2.3 shows the schematic of the hydrodynamic mechanical pulsator. It was designed to generate pressure fluctuations from the feed line to the injector. The propellant enters the hydrodynamic mechanical pulsator from the inlet port and the hydrodynamic mechanical pulsator delivers the propellant to the injector through the outlet port. During this delivery, part of the propellant is divaricated to the connector when the connector coincides with the hole in the rotating disk. The connectors were made of Teflon to minimize the friction between the connector face and the rotating disk. Furthermore, this separated portion of the propellant is discharged through the waste port, generating a sinusoidal pressure fluctuation in the feed line. The amount of the separated portion can be controlled by throttling the connector cross-section area with the throttle valve shown in Fig. 2.4 or by changing the pressure drop between the hydrodynamic mechanical pulsator and the waste port by adjusting the backpressure of the rotating disk. The hydrodynamic mechanical pulsator can generate pressure fluctuations without influencing the working fluid. Fig. 2.5 is the rotating disk of the hydrodynamic mechanical pulsator. There are 20 holes with 12 mm of diameter located circumferentially at the perimeter of the disk. The hole in the rotating disk has diverging contour to assist the smooth discharge of the test fluid. The driving motor is a 3 HP 3-phase induction motor with inverter to change the rotation speed of the shaft to desired RPM. The changeable RPM range of the motor is up to 3500 RPM and the motor RPM is monitored with a proximity sensor in Fig. 2.6. The combination of the motor and the rotating disk can generate the pressure pulsation with the frequency range of 1,000 Hz. This device was designed to work under the conditions of an internal pressure up to 50 bars for utilization in experiments with high pressure vessel. Coolant passage in Fig. 2.7 were installed for the high pressure mechanical sealant.

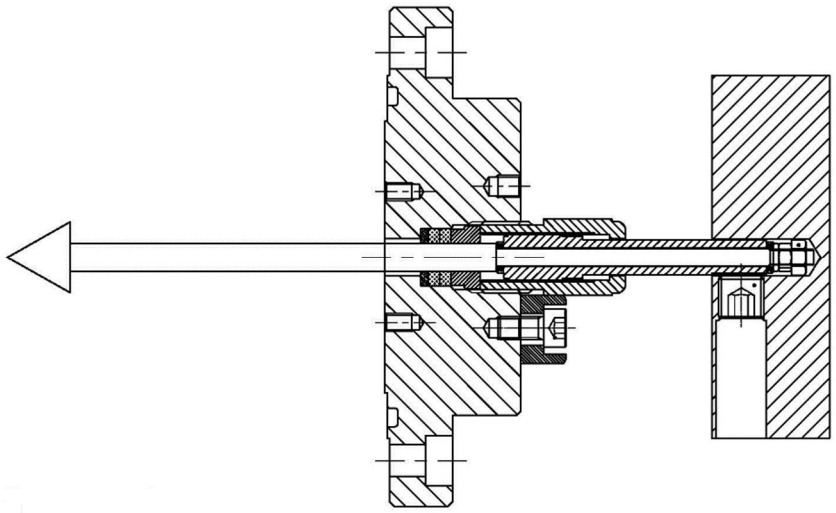

Fig. 2.4 Throttle valve in hydrodynamic mechanical pulsator.

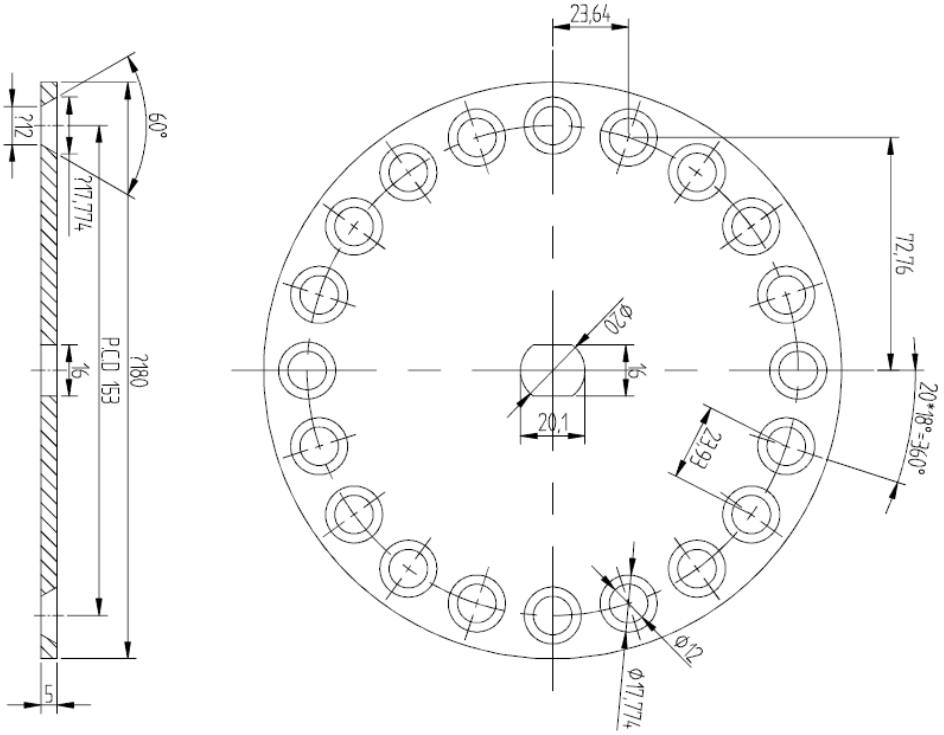

Fig. 2.5 Rotating disk in hydrodynamic mechanical pulsator.

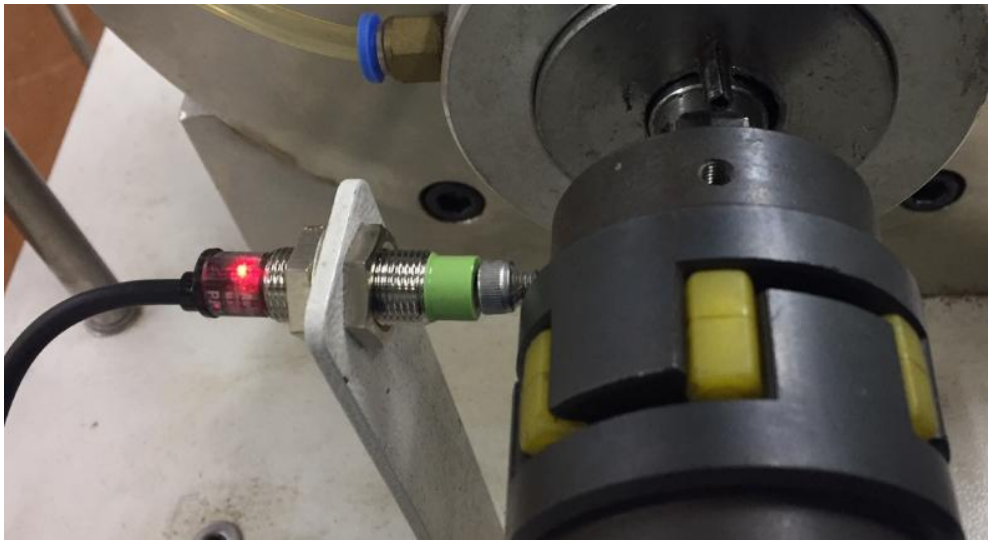

Fig. 2.6 Proximity sensor in hydrodynamic mechanical pulsator.

Fig. 2.7 Coolant passage in hydrodynamic mechanical pulsator.

Fig. 2.8 shows the amplitudes of the feed line pressure fluctuations throughout the operational pulsation frequencies. The amplitudes do not vary much in most of the frequencies, which means that the hydrodynamic mechanical pulsator designed and manufactured for this study delivers pressure pulsation effectively throughout the frequencies used in the experiment. The liquid film thickness amplitudes measured in the experiment were normalized with these feed line pressure amplitudes.

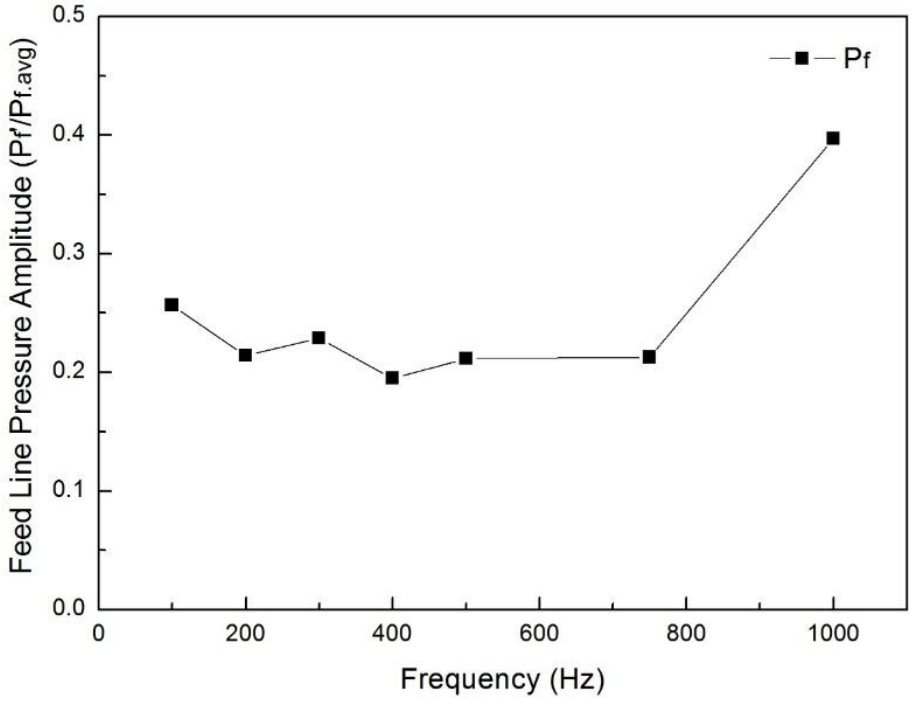

Fig. 2.8 Frequency–amplitude diagram of pressure in the feed line.

2.3 Electric conductance method

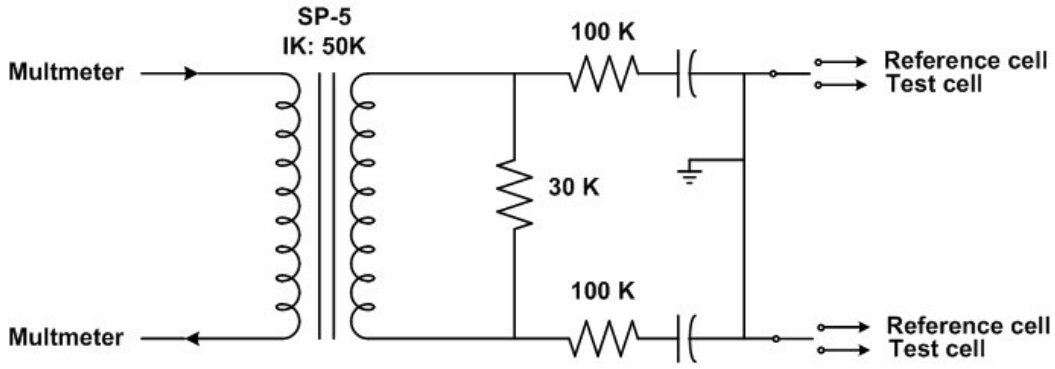

Fig. 2.9 Conductivity drive circuit (ref. [21]).

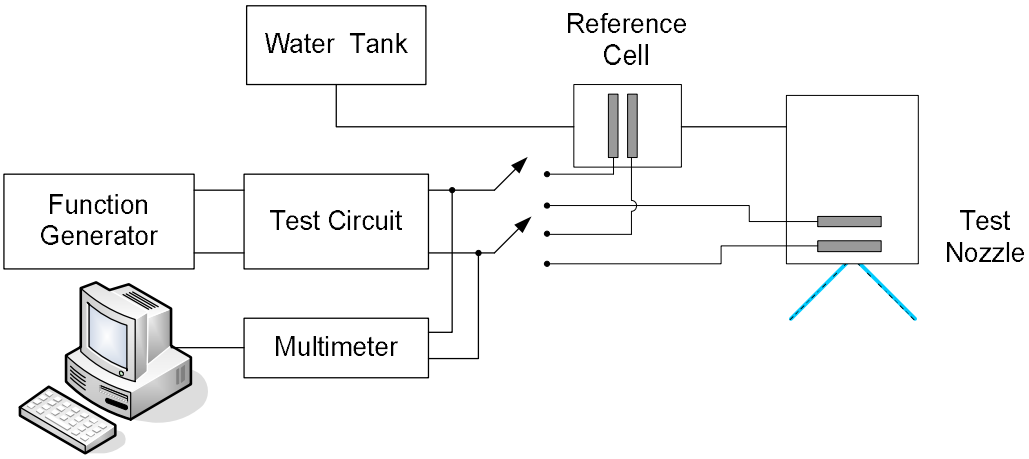

Fig. 2.10 Apparatus for liquid film thickness measurement (ref. [22]).

Measurement of thickness in ring-shaped liquid film has been done with electric conductance between 2 electrodes suggested by Suyari and Lefebvre in 1986.[21] The electric conductance is the ease with which an electric current passes the material. The inverse quantity is electrical resistance. The SI unit of electrical conductance is siemens, S. The electrical conductance between 2 separated electrodes is determined by the thickness of the water that connects the electrodes while running through them. This method has been widely used in various experiments and proven to be reliable.[4, 5, 12, 14, 16, 21, 23-26] The electrodes are connected to the test circuit shown in Fig. 2.9. The power source of the test circuit is a function generator which gives sinusoidal voltage input of 10 kHz with the peak to peak amplitude of 20 V. The electrical conductance of the liquid film between the electrodes also varies by the temperature. To compensate the influence of the temperature, reference cell is installed in the feed line. The schematics of the electrical conductance measurement system is shown in Fig. 2.10. The sectional view schematic of the device is shown in Fig. 2.11. The electrodes made of titanium and the insulators made of Teflon are put together with non-conductive adhesive. The thickness of titanium electrodes is 0.3 mm and the thickness of Teflon insulators is 0.5 mm. The body of the device was made of Polyether-ether-ketone (PEEK). The relation between the voltage and the liquid film thickness is determined through calibration with acrylic sticks of several different diameters inserted into the injector exit which are shown in Fig. 2.12. When the liquid is filled with the acrylic sticks inserted, the thickness of the liquid film is known. Measured voltage at the time can be collected to calibrate the voltage-liquid film thickness relation. Fig. 2.13 shows a calibration result for one of the device manufactured for the experiment. This calibration curve was obtained for each electrode device with different orifice diameters. Once the calibration was complete, the electrode device was installed at the exit of the swirl injector. Fig. 2.14 shows the detailed thickness of the plates stacked in the device. The liquid film thickness measured during the experiments is measured at approximately 1.45 mm upstream from the injector exit tip.

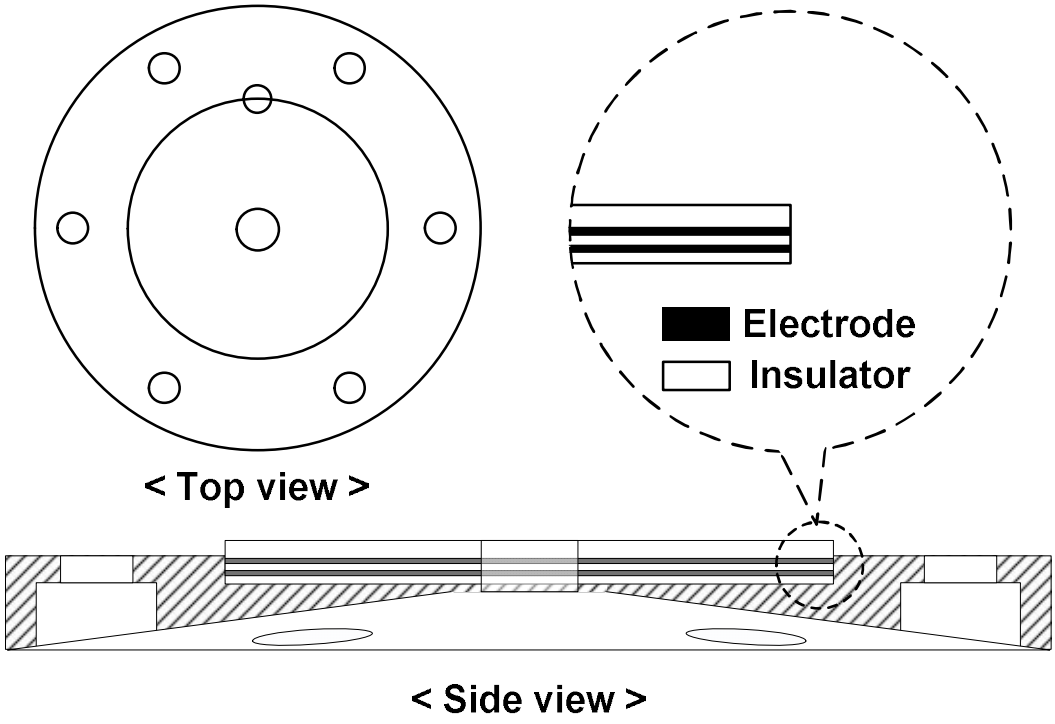

Fig. 2.11 Schematics of the electric conductance method.

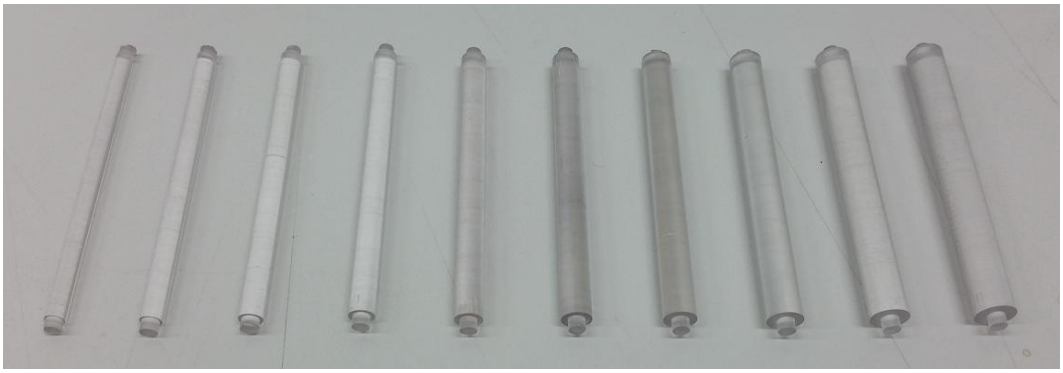

Fig. 2.12 Acrylic sticks of varying diameters for calibration.

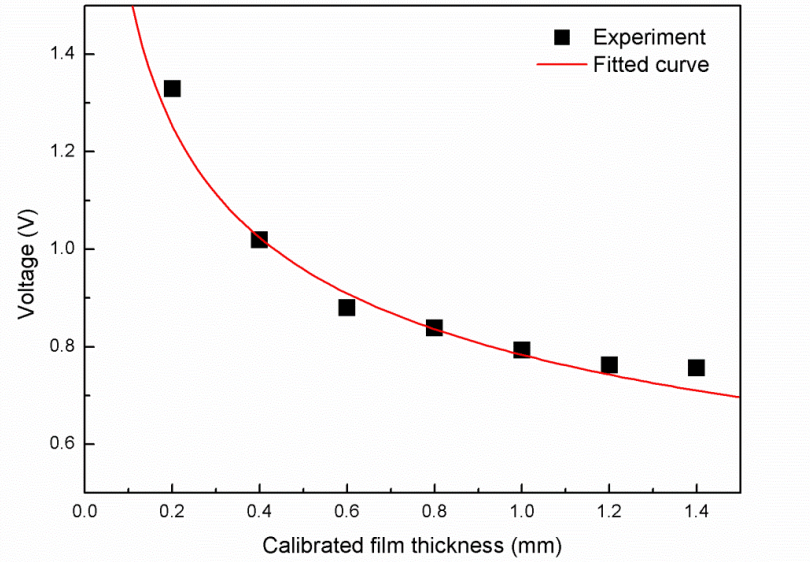

Fig. 2.13 Calibration result of a liquid film thickness measurement device.

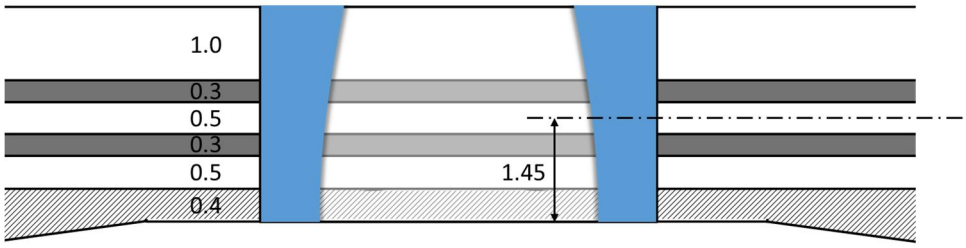

Fig. 2.14 Detailed thickness of electrode and insulator. (in mm)

2.4 Experimental apparatus and conditions

Experiments to investigate the dynamic characteristics of swirl injectors were conducted with water as the test fluid. Figure 2.15 shows the schematics of the experimental apparatus. An air compressor that can pressurize the air up to 100 bar was connected to high pressure water tank. The pressure in the water tank was controlled with a feedback system to maintain desired pressure. The pressurized water was supplied to the hydrodynamic mechanical pulsator to generate sinusoidal pressure pulsation in the feed line. A by-pass line was installed at the hydrodynamic mechanical pulsator to stabilize the pressure pulsation. The pressure was measured with static pressure sensor and dynamic pressure sensor simultaneously at every measuring points. Feed line pressure, P_f was measured after the hydrodynamic mechanical pulsator with static pressure sensor (Valcom, VPRQ-A5-20Bar-4C) and dynamic pressure sensor (PCB, 101A04). Manifold pressure, P_m was measured at the manifold with static pressure sensor (Valcom, VPRQ-A5-20Bar-4C) and dynamic pressure sensor (PCB, 102B06). Orifice pressure, P_o was measured after the hydrodynamic mechanical pulsator with static pressure sensor (Valcom, VHR3-A5-2Bar-4C) and dynamic pressure sensor (PCB, 102M205). Electrodes to measure the reference and liquid film thickness were installed at the feed line and orifice respectively. Sampling rate for the pressure sensors and electrodes was 400 kHz.

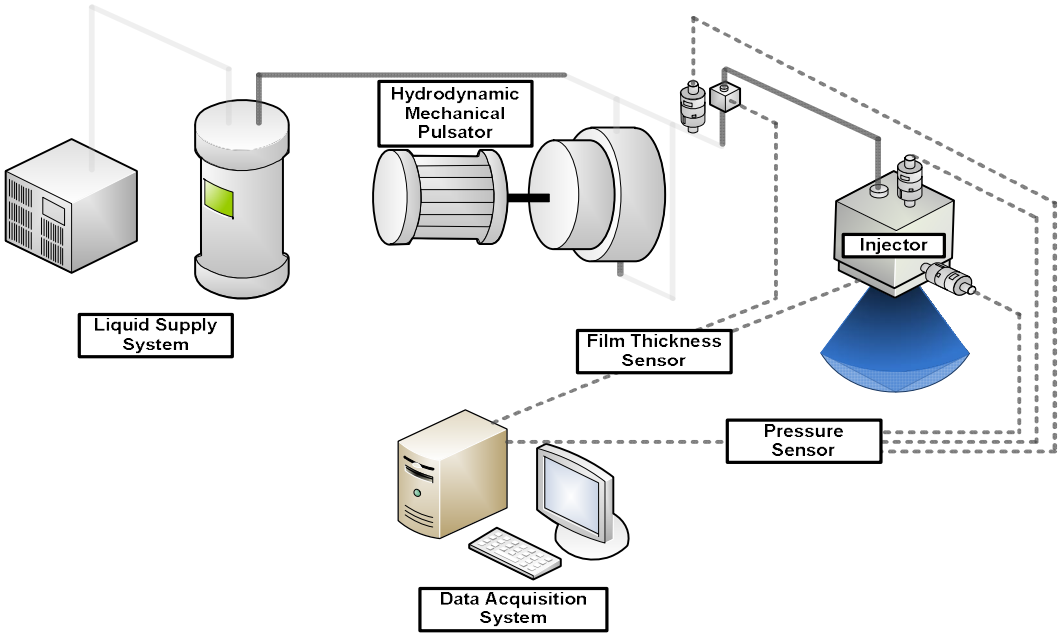

Fig. 2.15 Experimental Apparatus.

CHAPTER 3

DYNAMIC CHARACTERISTICS OF OPEN-TYPE SWIRL INJECTOR

3.1 Geometry of open-type swirl injector

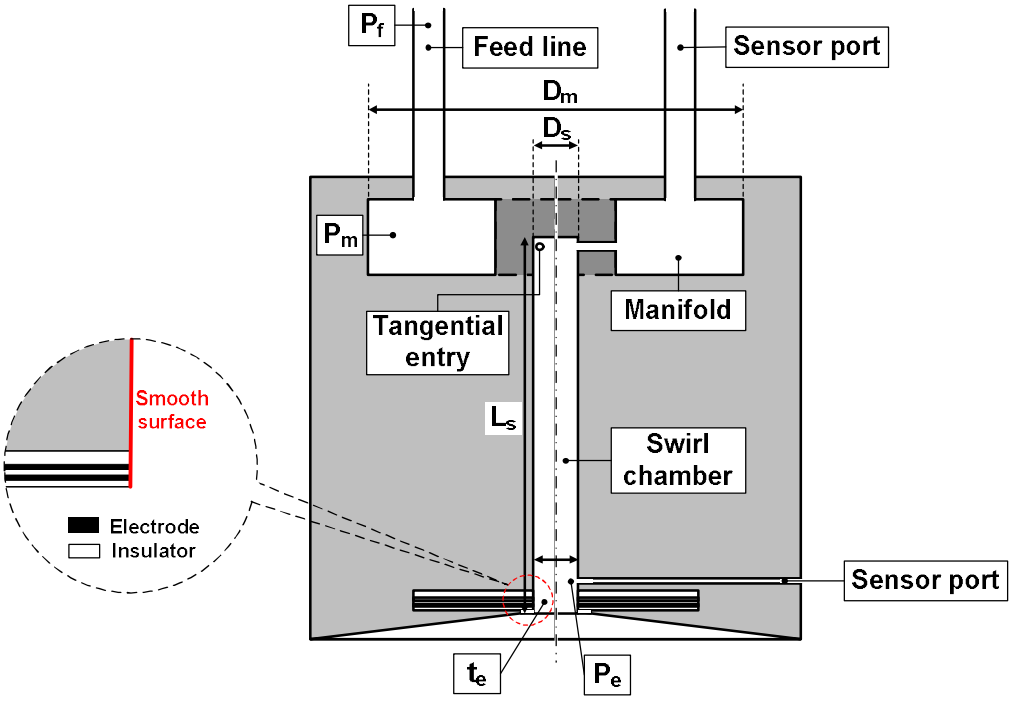

Fig. 3.1 Schematics of open-type swirl injector.

Table 3.1 Open-type swirl injector geometries.

D_m [mm]	n_t	L_s [mm]	D_s [mm]	L_s / D_s	A
50	3	55	6	9.17	4.69
			7	7.86	6.67
			8	6.88	8.98
			9	6.11	11.63
		50	7	7.14	6.67
		55		7.86	
		60		8.57	
		65		9.29	
44	3	55		7.86	
56	3				
50	2				
50	4				

Figure 3.1 shows the sectional view schematic of an open-type swirl injector designed for this study. The injector was designed with replaceable parts to change the length and the diameter of the swirl chamber, the number of tangential entries, and the diameter of the manifold. The injector body was made of polycarbonate (PC) which is a non-conductive material to avoid noise to the electrode that was installed to measure liquid film thickness. Table 3.1 shows the injector geometry parameters selected for the present study. Pressure sensors were installed at the feed line, manifold, and exit of the swirl chamber, which are denoted as P_f, P_m, and P_e, respectively, in Fig. 3.1. The subscript for orifice was replaced from o with e, since the open-type swirl injector does not have an orifice geometry. Electrodes to measure the liquid film thickness at the exit of the swirl chamber, which is denoted as t_e in Fig. 3.1, were installed at the end of the swirl chamber. The measuring point of the liquid film thickness was approximately 1.45 mm before the injector exit. The frequencies of the generated pressure oscillations in the feed line created by the hydrodynamic mechanical pulsator were 100–1,000 Hz. Fig. 3.2 shows the effect of different frequency intervals. Frequency interval was set to be 100 Hz in Fig. 3.2(a). To verify the interval was sufficient to describe the dynamic characteristics of the open-type swirl injector, the near peak region was subdivided in to 25 Hz intervals. The results are shown in Fig. 3.2(b). The dynamic characteristics changes linearly and does

not show any sudden peaks. Since additional frequencies require more time and resources, the adequate interval for open-type swirl injector was decided as 100 Hz. In addition, the average pressure level in the injector manifold was maintained at 4 bars.

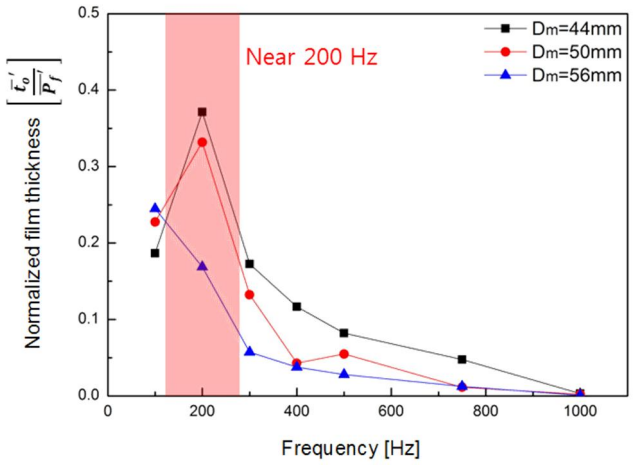

(a)

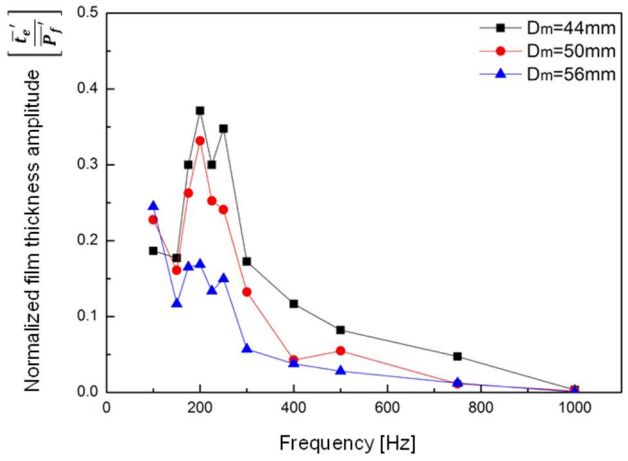

(b)

Fig. 3.2 Changes in dynamic characteristics with frequency intervals in open-type swirl injector.

3.2 Pressure at the swirl chamber exit

As the primary purpose of the injector is the stable delivery of the designed mass flow rate to the combustion chamber, the mass flow rate has been the major parameter in injector studies. Previous research on injector dynamics also focused on the stability of the mass flow rate by choosing it as the output parameter.[2, 5, 12] Khil derived an equation that calculates the instantaneous mass flow rate with the pressure and liquid film thickness measured at the injector orifice—the exit of the injector—which is called the Direct Pressure Measurement Method (DPMM).[12] This method has been verified to work well with closed-type swirl injectors. The two key parameters that determine the mass flow rate in this method are the axial velocity and the liquid film thickness at the injector exit. The axial velocity is calculated from the measured pressure in the injector exit, and the liquid film in the injector exit is directly measured using the electric conductance method. However, as there is no converging section in an open-type swirl injector, the pressure in the swirl chamber drops extremely fast, which causes the pressure sensor signal at the swirl chamber exit to be very low. The amplitudes of the pressure and the liquid film thickness at the swirl chamber exit in every tested injector and at every tested pulsation frequency are shown in Fig. 3.3. Compared to the amplitude of the liquid film thickness signal, the amplitude of the pressure signal is insignificant. This condition makes it impossible to apply DPMM to open-type swirl injectors to obtain an instantaneous mass flow rate. For this reason, the liquid film thickness was selected as the major output parameter, as it is the dominant parameter that well represents the output characteristics of the injector in this study.

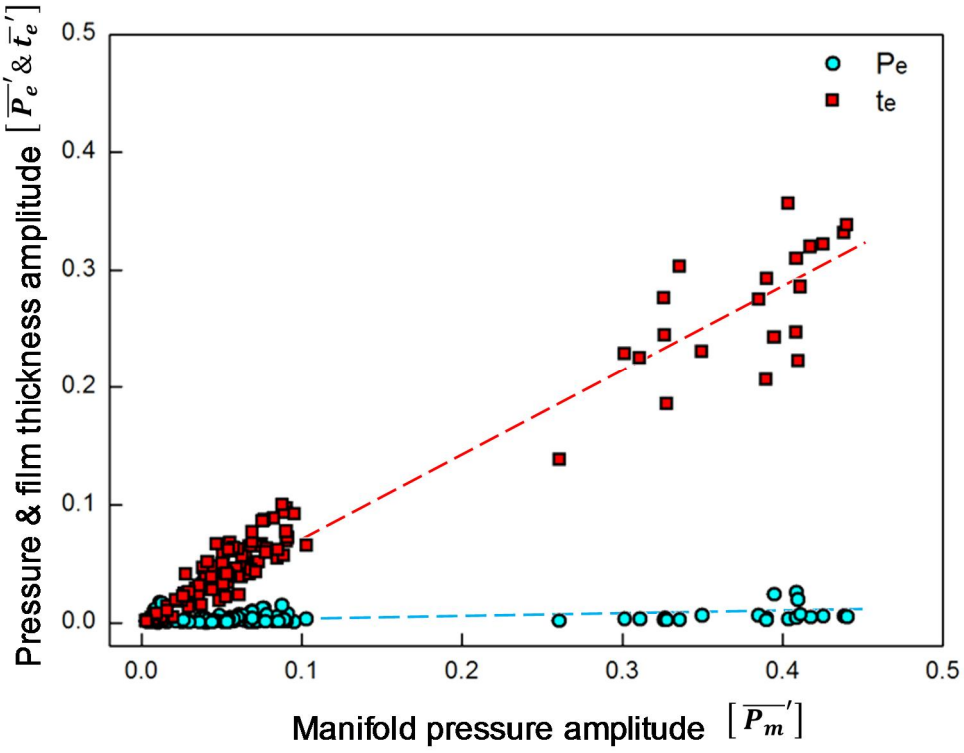

Fig. 3.3 Pressure and liquid film thickness amplitude at the swirl chamber exit.

3.3 Effects of swirl chamber length and diameter variation

A The fluctuation value was normalized with an average value to obtain fluctuation amplitudes. The relation between the manifold pressure and the liquid film thickness at the swirl chamber exit were analyzed. Fig. 3.4 shows the result. The x-axis represents the manifold pressure amplitude, while the y-axis represents the liquid film thickness amplitude at the swirl chamber exit. These plots show the relation in that the liquid film thickness amplitudes are proportional to the manifold pressure amplitude. However, the average slope between the manifold pressure and liquid film thickness amplitude depends on the swirl chamber length diameter of the injector, on which this section is focused.

To observe the influence of the swirl chamber length on the injector's dynamic performances, a series of experiments were performed at swirl chamber lengths of 50 mm, 55 mm, 60 mm, and 65 mm with a constant swirl chamber diameter of 7 mm. It is shown in Fig. 3.4(a) that the average slope of each case increased as the swirl chamber length decreased. This type of figure demonstrates the dynamic sensitivity of the injector to the overall frequencies of disturbances. A smaller slope means less sensitivity to disturbances, which is a favorable characteristic for an injector. It is believed that the reason for this tendency is energy loss by the friction force as well as the damping effect of the wave itself due to the longer residence time of the propellant inside the swirl chamber. As the residence time is increased due to a longer swirl chamber, the energy traveling with the wave propagation is dissipated, reducing the wave amplitude initiated by the disturbance.

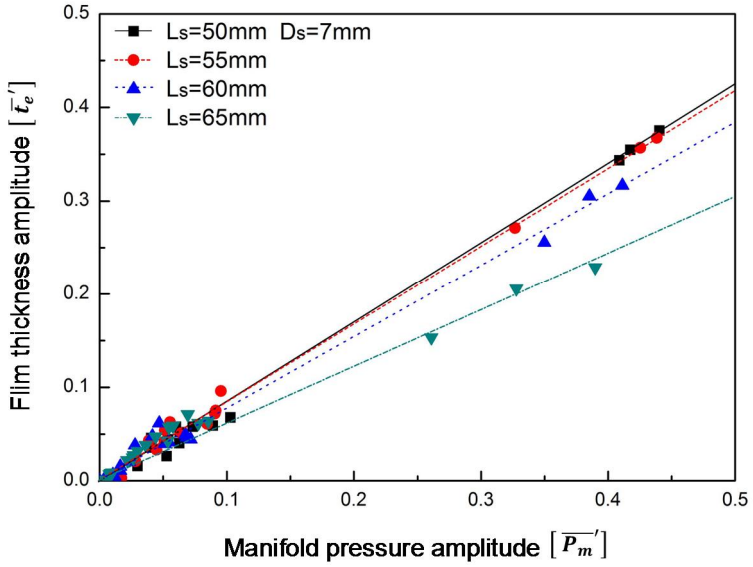

(a)

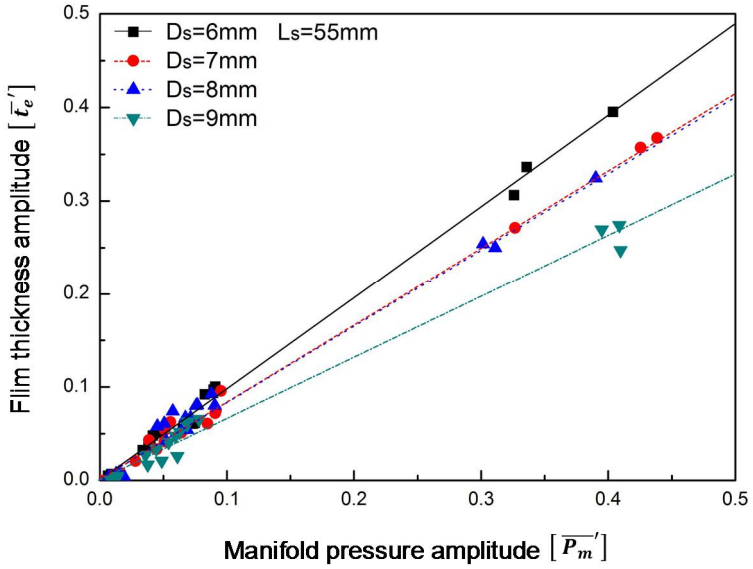

(b)

Fig. 3.4 Relation between manifold pressure and liquid film thickness amplitude for a) swirl chamber length variation and b) swirl chamber diameter variation.

Figure 3.4(b) illustrates the result of the experiments that were conducted to investigate the influence of the swirl chamber diameter on the injector's dynamic performances. The diameter of the swirl chamber varied from 6 mm to 9 mm at a 1-mm interval. The slope between the input and output amplitudes of the swirl chamber diameter variation increased as the swirl chamber diameter decreased. This result can be explained by focusing on the initial wave, which is delivered into the swirl chamber through the tangential entry. The amplitude of the surface wave in the swirl chamber is determined as follows [2, 17]:

$$\bar{\Omega} = \frac{1}{A\sqrt{2(\bar{R}_s^2 - a)}} \frac{v_t'}{v_t} \tag{3.1}$$

Where the geometric characteristic parameter A is defined as

$$\mathrm{A} = \frac{(R_s - R_t)R_0}{nR_t^2} = \frac{\text{tangential velocity} \times \text{arm coefficient}}{\text{axial velocity}} \tag{3.2}$$

And the normalized swirl chamber radius $\bar{R}_s$ is defined as

$$\bar{R}_s = \frac{R_s}{R_o} \tag{3.3}$$

There is no converging section in an open-type swirl injector, Ro=Rs. Therefore, the amplitude of the surface wave will increase with a decreasing swirl chamber diameter, which coincides with the experimental data. This is because geometric characteristic parameter A decreases with a decreasing swirl chamber diameter.

The relationship between the pulsation frequency and fluctuation amplitude of the liquid film thickness at the swirl chamber exit was also investigated. This frequency–amplitude analysis is conducted to investigate the injector's response to individual frequencies of disturbances, while a relation analysis between the manifold pressure and liquid film thickness at the swirl chamber exit was conducted to investigate the average response to all frequencies of the disturbances given in this experiment.

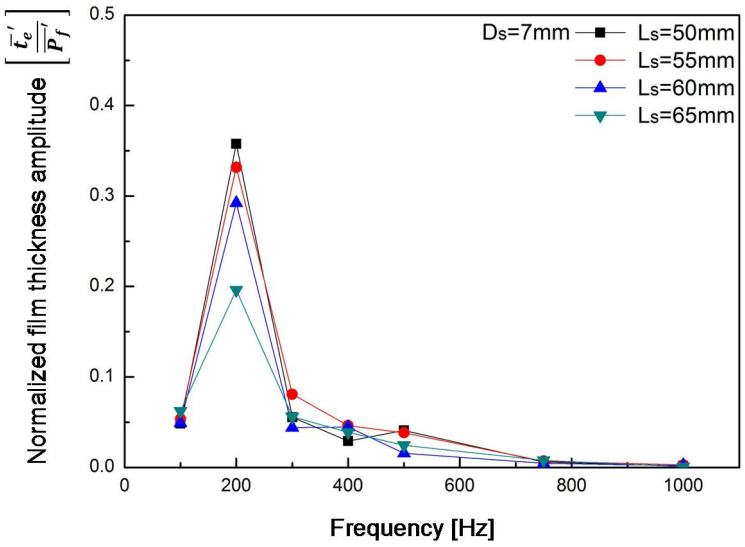

(a)

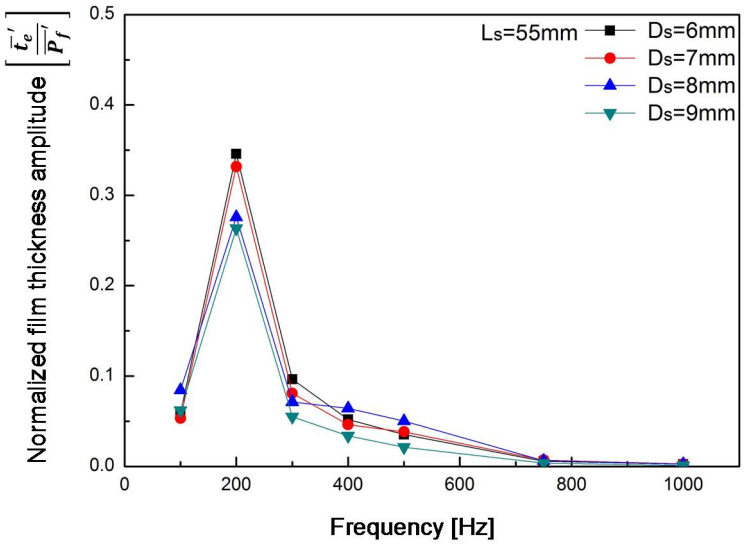

(b)

Fig. 3.5 Frequency–amplitude diagram of liquid film thickness amplitude for (a) swirl chamber length variation and (b) swirl chamber diameter variation.

Figures 3.5(a) and 3.5(b) show the results of the swirl chamber length variation and diameter variation, respectively. The amplitudes of the liquid film thickness fluctuations increase with pulsation frequency increases at the initial part of the frequency range, forming the maximum peak at a frequency of 200 Hz. Then, the amplitude of fluctuation reduces drastically with a pulsation frequency rise of up to 1,000 Hz. Every injector used in the experiment on swirl chamber length and diameter variation had the same tendency. Figure 3.5(a) shows the result of the fluctuation amplitude being decreased by increasing the swirl chamber length, while Fig. 3.5(b) shows the effect of the swirl chamber diameter, where the fluctuation amplitude of the liquid film thickness is decreased as the swirl chamber diameter is increased. This result provides important information for designing an open-type swirl injector. Within the frequency range of this study, open-type swirl injectors designed for swirl chamber length and diameter variation studies show distinct weak points in dynamic stability around a frequency of 200 Hz. It also provides information on how to deal with the amplitude of fluctuation by changing the injector geometry. With a larger diameter and a longer length of the swirl chamber, the disturbances at the peak can be dampened.

However, the maximum peak frequency at 200 Hz did not change despite the change in the swirl chamber length from 50 mm to 65 mm and in the swirl chamber diameter from 6 mm to 9 mm. When Bazarov suggested the importance of an injector's dynamic characteristics in the 1970s, he provided the example of a typical closed-type swirl injector's output parameter amplitude in a frequency domain that had a peak in the moderate range of 100–300 Hz and showed a rapid decrease as the frequency increased.[2] After his efforts, different output parameter peaks with various injector geometries were reported throughout the world. Marchione et al. detected the spray cone angle peak and mie scattering signals at approximately 100 Hz in a closed-type swirl injector without causing external disturbances.[27] Khil et al. verified the peak of the output parameter at 250 Hz with pulsation in a closed-type swirl injector.[5] As well, Ismailov et al. calculated approximately a 200-Hz peak of a closed-type swirl injector by applying

Bazarov's theory.[8, 9]

However, most of these research examples focused on measuring and analyzing the dynamic characteristics of the injector itself rather than deriving the physical reason for the dynamic instability peaks. Among the works, Ismailov et al. modified Bazarov's equations and suggested the reflected wave that is produced due to the converging section in the closed-type swirl injector was the reason for the fluctuation amplitude peak of the injector. However, this converging section does not exist in the open-type swirl injector. From the inspiration of Ismailov et al.'s work, we took notice of the injector manifold and tangential entry, which is the only converging section that exists in an open-type swirl injector. Additional parts were manufactured and experiments were conducted to investigate the influence of the injector manifold and tangential entry. The result is discussed in later section of the paper.

3.4 Dynamic characteristics in low frequency region

Since the open-type swirl injector's structure is a simple cylinder after the tangential entry, the whole open-type swirl injector's dynamic characteristic is supposed to be following the tangential entry's transfer function and theoretical previous works show results that is similar to the tangential entry transfer function.[17] An theoretical transfer function of tangential entry from Bazarov's theory is shown below.[2]

$$\begin{cases} Re\Pi_{\tau} = 1/2\,(1 + Sh_{\tau}^{2})\,; \\ Im\Pi_{\tau} = -Sh_{\tau}/2(1 + Sh_{\tau}^{2})\,; \end{cases} \tag{3.4}$$

Calculated result from eq. 3.4 with an open-type swirl injector case is shown in Fig. 3.6. The magnitude of the transfer function decreases monotonously as the pulsation frequency is increased. The experimental result on the dynamic characteristic of the open-type swirl injector is shown in Fig. 3.7. The dynamic characteristic shows same monotonous decreasing tendency above the pulsation frequency of 200 Hz. However, the experimental result under 200 Hz of pulsation frequency shows increasing tendency with pulsation frequency increase which is the opposite from the known analytical results.

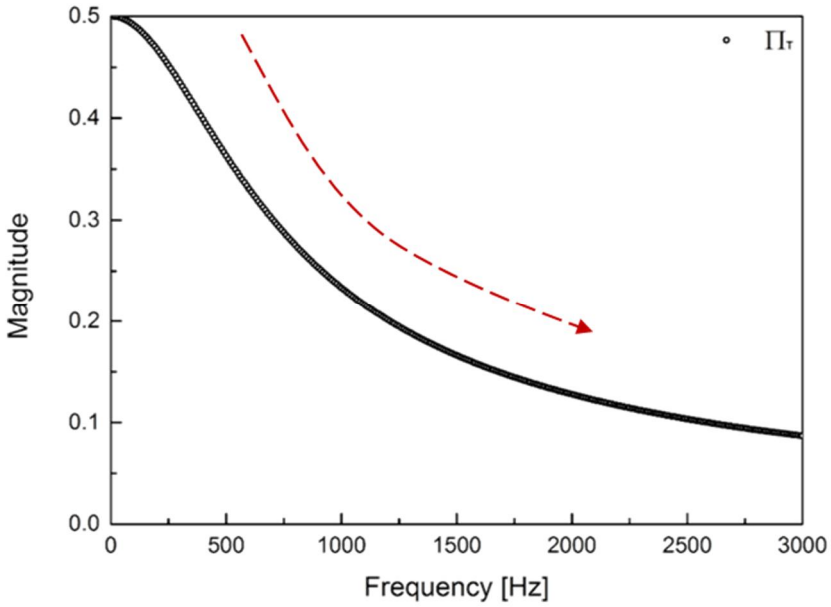

Fig. 3.6 Tangential entry transfer function of open-type swirl injector.

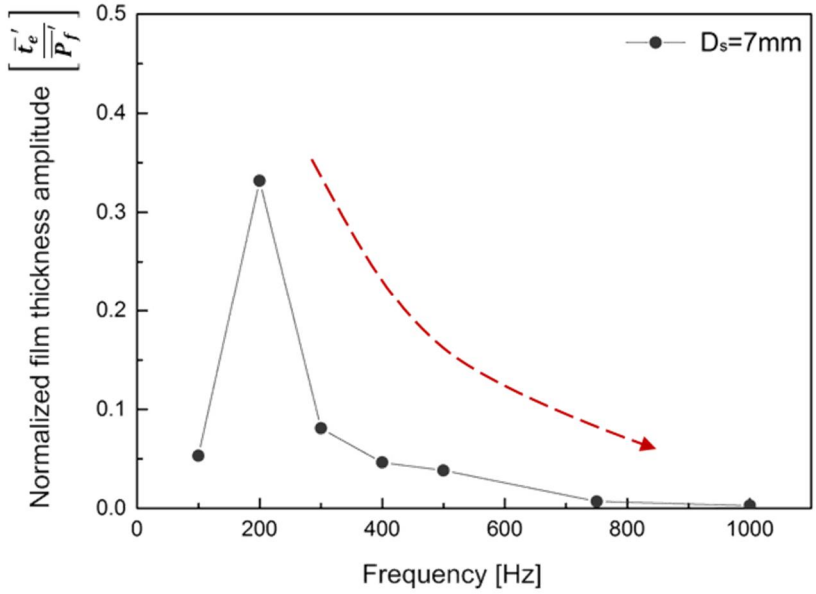

Fig. 3.7 An experimental result of open-type swirl injector's dynamic characteristics.

The first approach for the reason of 200 Hz peak was to verify if it is an effect of resonance in the manifold. Fig. 3.8 is a simplified schematic of pulsator-injector connection. Every component is symbolized as a cavity or a simple pipe. From this view, the only diverging-converging section is the manifold and tangential entry. Since it was supposed as a resonance in the manifold, geometry of manifold and tangential entry were varied to verify its influences on the dynamic characteristic result through experiment. The experimental results of open-type swirl injector's dynamic characteristics are shown in Fig. 3.9 with varying (a) manifold diameter, (b) manifold height, and (c) tangential entry length. All three cases of injector geometry variations did not show frequency change of the peak in 200 Hz region. A resonance should change its frequency within the change of geometry. The first hypothesis found out to be far from the real physics.

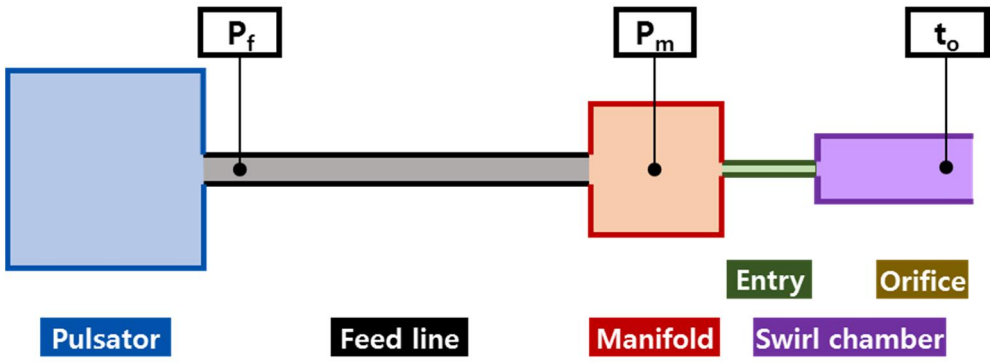

Fig. 3.8 Simplified schematic of pulsator-injector connection.

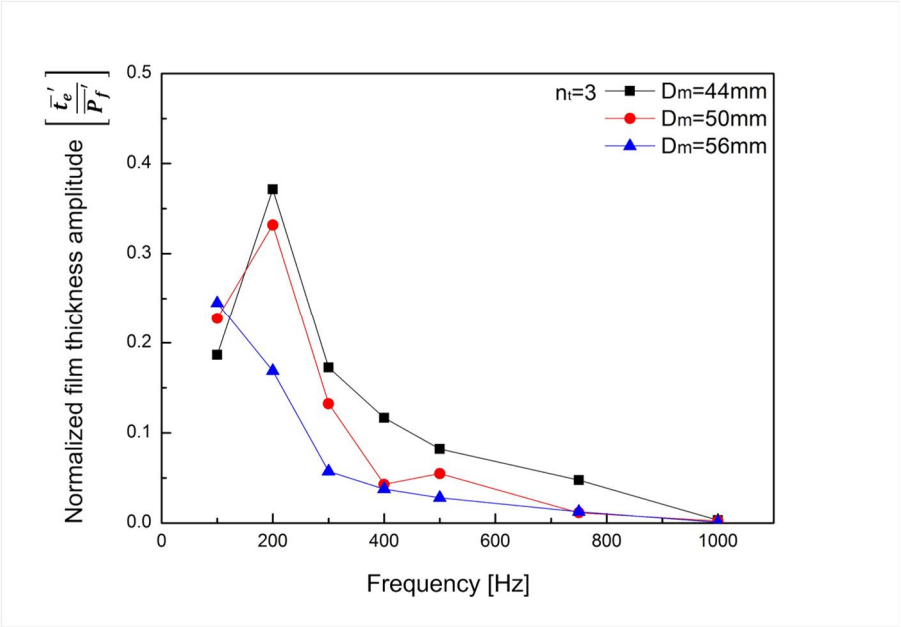
Normalized film thickness amplitude $\left[\frac{\overline{t_e}'}{\overline{P_f}'}\right]$
Frequency [Hz]
nt=3
Dm=44mm
Dm=50mm
Dm=56mm
0.0
0.1
0.2
0.3
0.4
0.5
0
200
400
600
800
1000

(a)

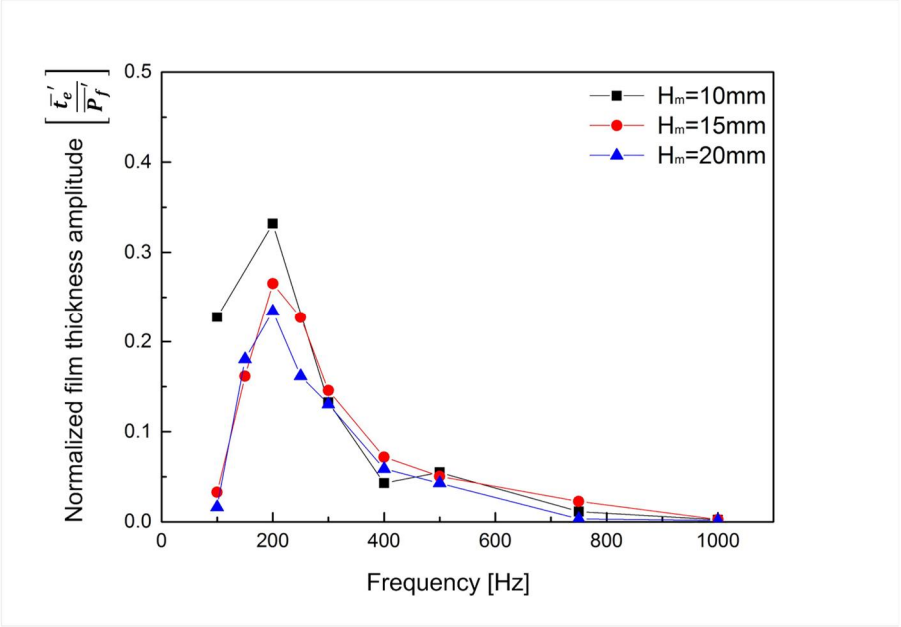
Normalized film thickness amplitude $\left[\frac{\overline{t_e}'}{\overline{P_f}'}\right]$
Frequency [Hz]
Hm=10mm
Hm=15mm
Hm=20mm
0.0
0.1
0.2
0.3
0.4
0.5
0
200
400
600
800
1000

(b)

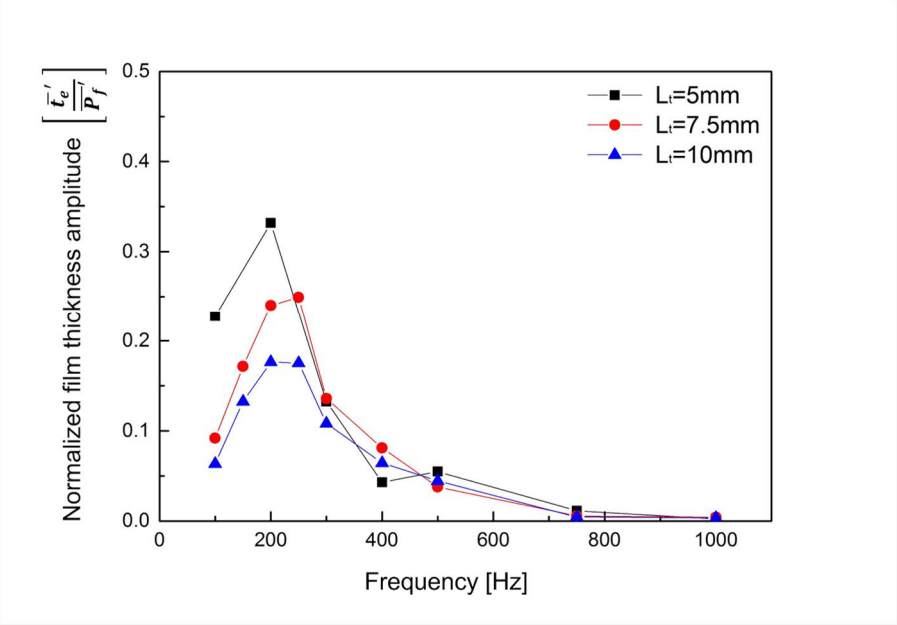

(c)

Fig. 3.9 Frequency–amplitude diagram of liquid film thickness amplitude for (a) manifold diameter variation and (b) manifold height variation (c) tangential entry length variation.

A second approach was done. Fig 3.10 is the measured manifold pressure of open-type swirl injector with 100 Hz and 200 Hz pulsation frequencies. The 200 Hz result shows a fine sinusoidal oscillation but the 100 Hz result shows a rather distorted sinusoidal oscillation. The fast Fourier transform results of the measured manifold pressures are shown in Fig. 3.11. The 200 Hz result in Fig. 3.11(b) shows the 200 Hz peak which is the frequency it is excited. However, the 100 Hz result in Fig. 3.11(a) shows 200 Hz peak larger than the 100 Hz peak which is the frequency it is excited. To investigate the reason for this phenomenon, a simple experiment was done. Fig. 3.12 shows the experimental setup for the experiment. The feed line pressure and manifold pressure were measured while the length of the feed line between them is varied by 0.7 m, 1.0 m and 1.5

m with the pulsation frequency of 100 Hz. The measured pressures are shown in Fig. 3.13. The feed line pressure of each feed line length case show fine 100 Hz signals. This result proves that the hydrodynamic mechanical pulsator itself is generating the exact desired pulsation frequency. On the other hand, the manifold pressure results show distorted signals with different shapes varying by the feed line length. To verify the reason of this distortion, supplement experiment was done. The experimental setup is shown in Fig. 3.14. The open-type swirl injector was removed from the setup and the manifold pressure sensor was installed at the end of the feed line. Without the open-type swirl injector, the distortion in the manifold pressure is gone as shown in Fig. 3.15. Since the distortion disappears without the open-type swirl injector, distortion originates from the open-type swirl injector. And with the result that the shape of the manifold pressure signal distortion varied when the length of the feed line was changed, it seems to be the interference of pressure wave that travels down the feed line and the reflected pressure wave from the injector geometry. Fig. 3.16 shows the schematics of superposition between the incident wave and the reflected wave. Based on the superposition theory, the manifold pressure signals were synthesized theoretically with varying phase difference due to the feed line length variation. The theoretical result and the experimental result are shown in Fig. 3.17. From this point of view, opposite tendency of low frequency region can be explained. Since the interference results from the converging geometry between the manifold and tangential entry, the maximum point at 200 Hz will be referred as 200 Hz peak in the paper for convenience even though it is not originated from resonance.

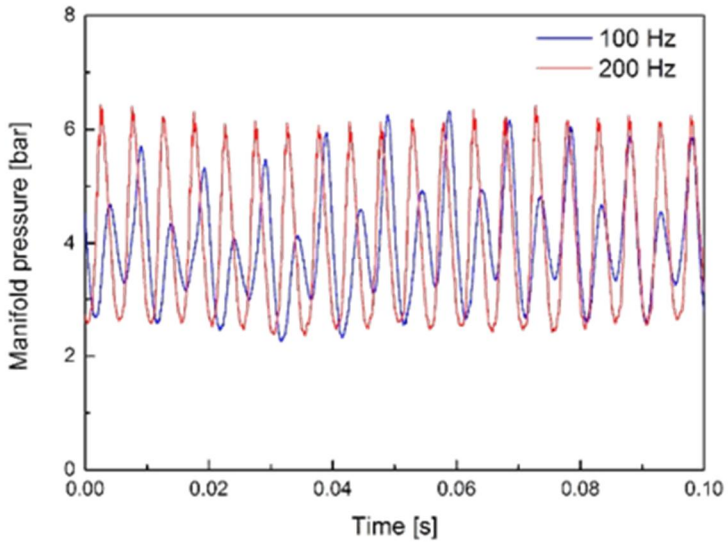

Fig. 3.10 Manifold pressure with pulsation frequency of 100 Hz and 200 Hz.

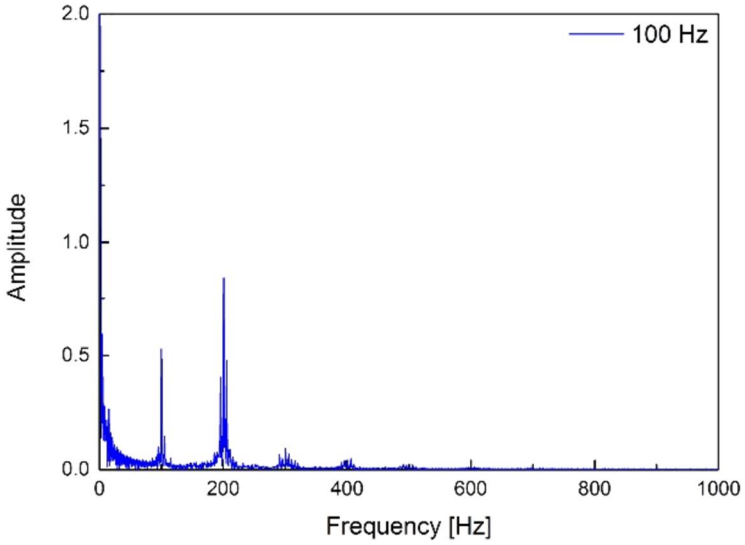

(a)

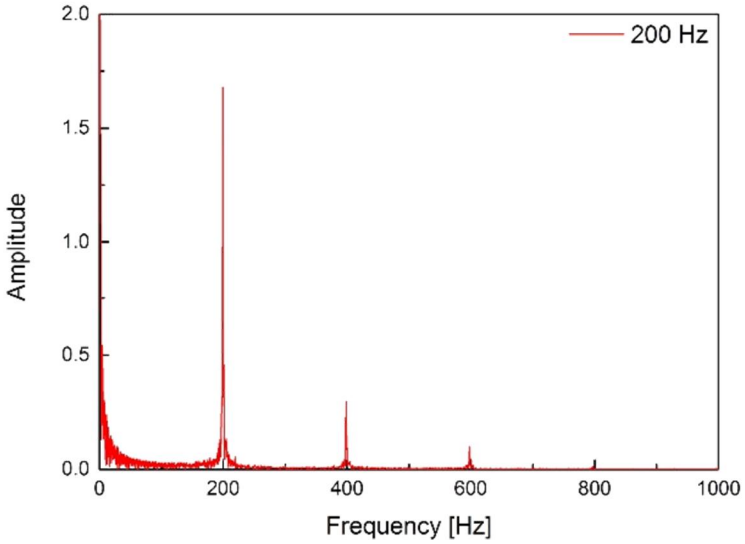

(b)

Fig. 3.11 FFT results for manifold pressure (a) 100 Hz (b) 200 Hz.

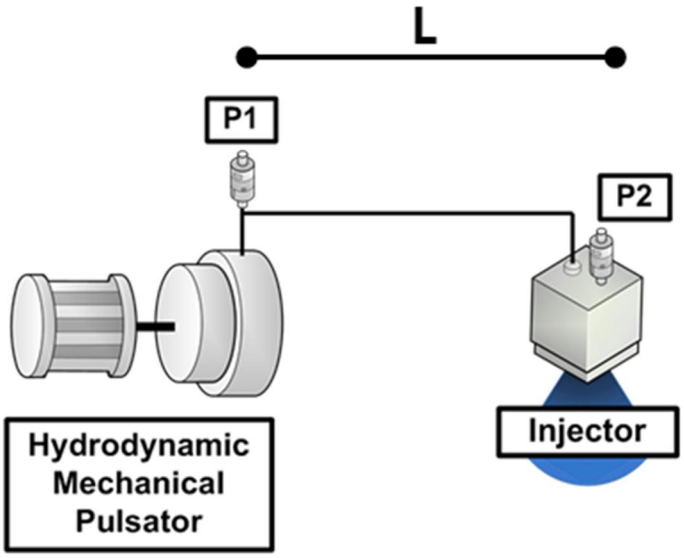

Fig. 3.12 Experimental setup.

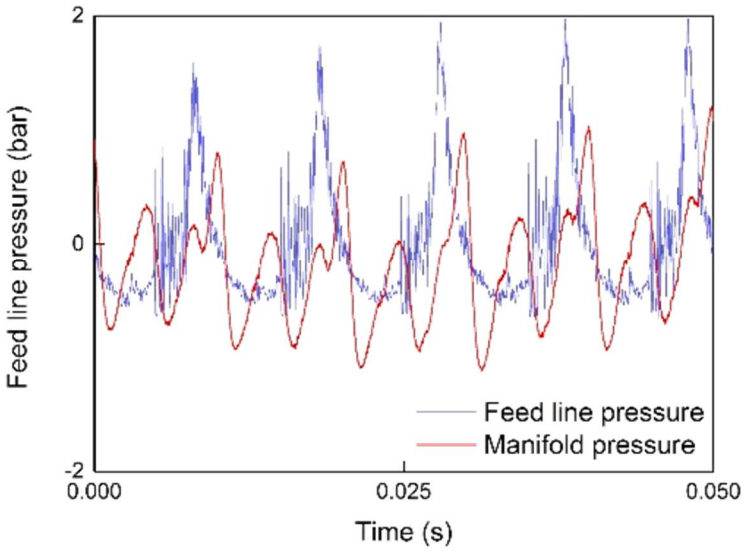

(a)

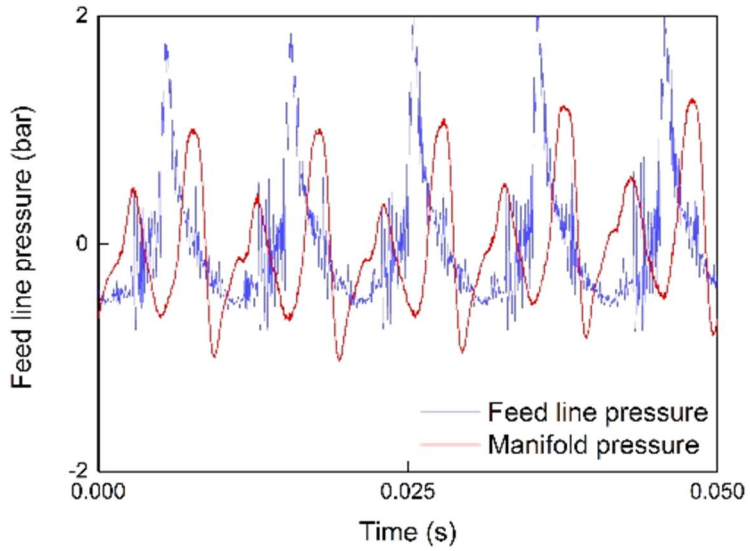

(b)

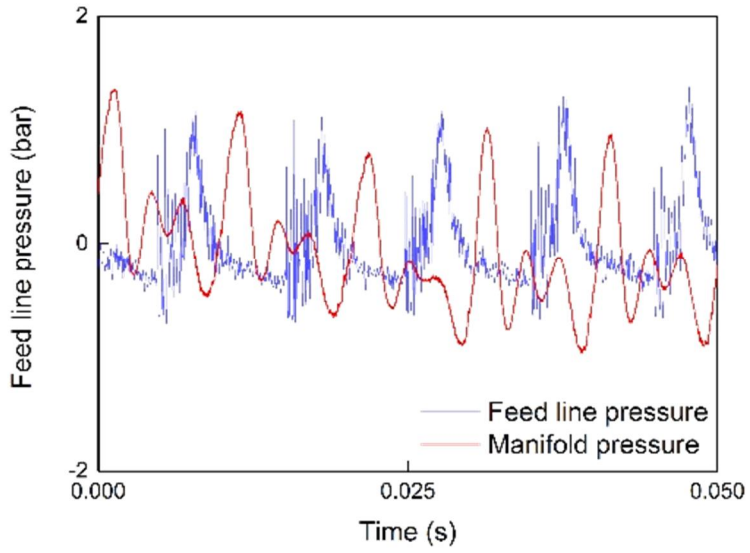

(c)

Fig. 3.13 Pressure signals with varying feed line length (a) 0.7 m (b) 1.0 m (c) 1.5 m.

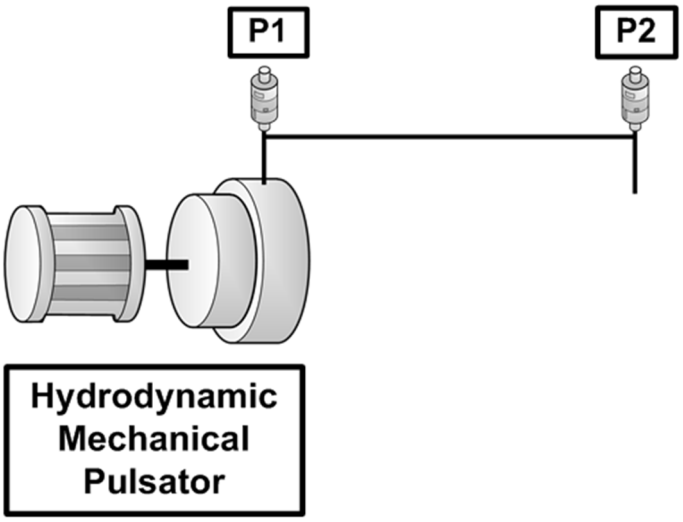

Fig. 3.14 Experimental setup.

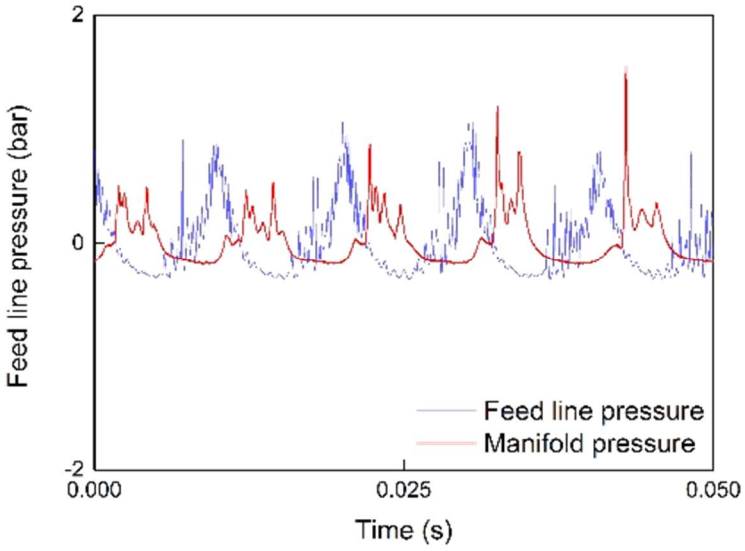

Fig. 3.15 Pressure signals without injector.

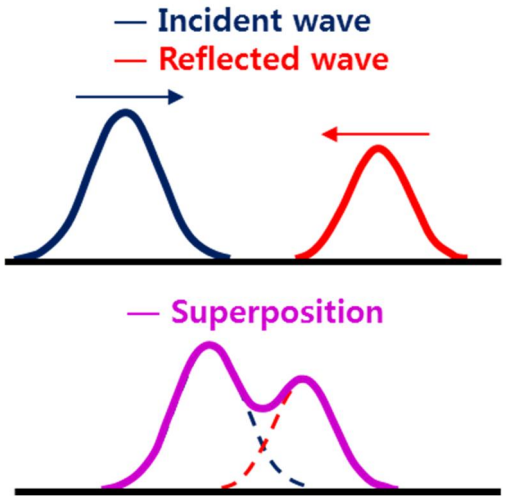

Fig. 3.16 Superposition between incident wave and reflected wave.

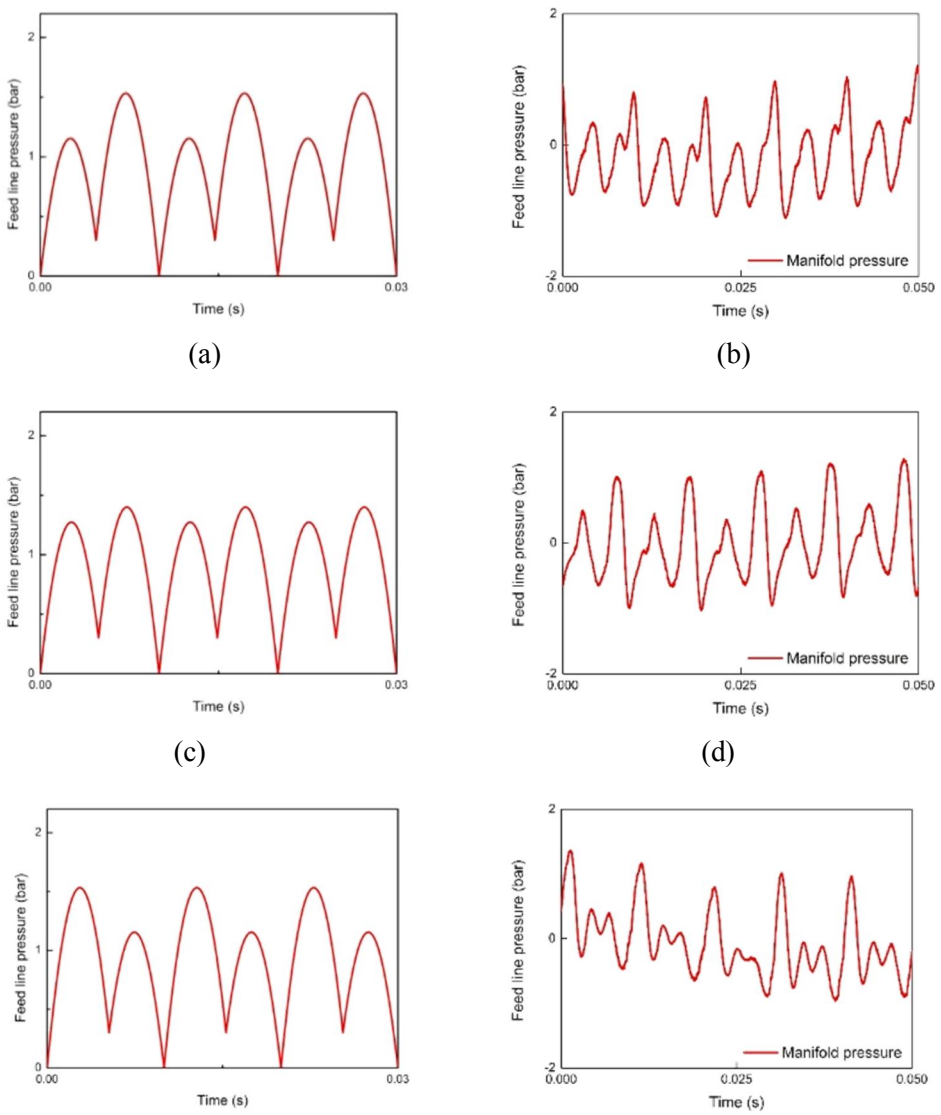

Fig. 3.17 Manifold pressure signals with varying feed line length (a) 0.7 m, theoretical (b) 0.7 m, experimental (c) 1.0 m, theoretical (d) 1.0 m, experimental (e) 1.5 m, theoretical (f) 1.5 m, experimental.

3.5 Spray cone angle

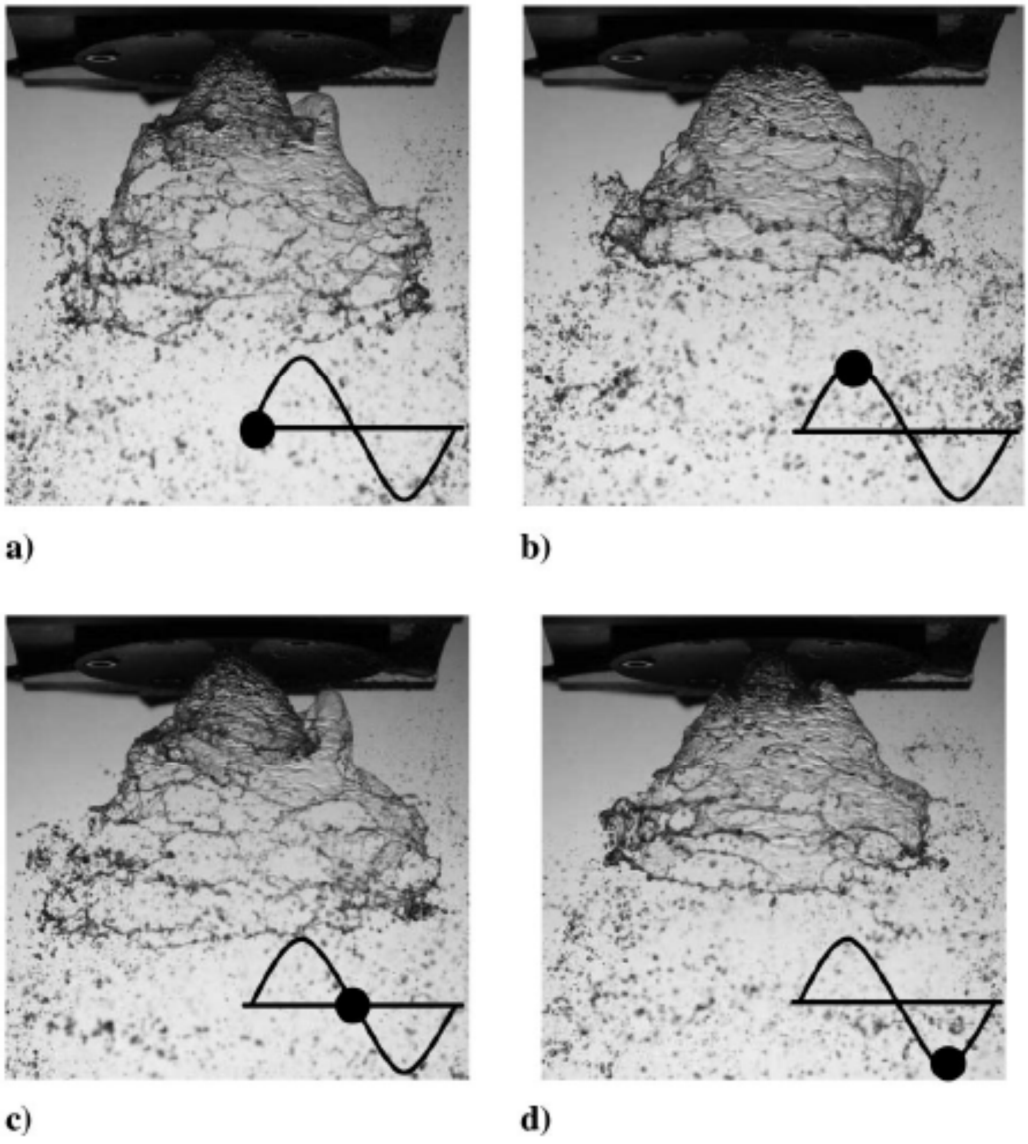

Fig. 3.18 Dynamic spray patterns of an open-type swirl injector during one cycle at a pulsation frequency of 200 Hz; (a) 0°; (b) 90°; (c) 180°; and (d) 270°

Instant spray images of an open-type swirl injector at a pulsation frequency of 200 Hz were taken, and four images representing each phase in one cycle are shown in Fig. 3.18. As the fluctuation of pressure pulsation is delivered, the spray cone angle is fluctuated with it. The spray cone angle is at its maximum, as shown in Fig. 3.18(b), and minimum, as shown in Fig. 3.18(d), in one cycle. Due to this spray cone angle change, the folded region of the spray surface is formed near the injector exit and it runs down as the propellant travels downstream. From the images taken throughout the experiment, the instantaneous spray cone half angle θ was measured at $1D_s$ downstream from the injector exit. Spray cone half angles that result in pulsation frequencies of 100, 200, 300, and 400 Hz are shown in Fig. 3.19. The result shows the same trend as the liquid film thickness amplitude results shown in Fig. 3.5. The average spray cone angle is approximately 35° throughout the pulsation frequencies, and the spray cone half angle fluctuates, with the largest range at 200 Hz. The injector demonstrates the greatest output fluctuations in both observations of liquid film thickness and spray cone angle measurements. In addition, this fluctuation peak at 200 Hz can be coupled with any other disturbance in the liquid rocket engine causing combustion instability. Therefore, suppressing the output parameter fluctuation peak or the liquid rocket engine with an operation range far from the peak frequency is a common method in liquid rocket injector design. Therefore, the objective of this study should be the detection of the fluctuation peak of the injector, as well as suggestions for ways to suppress the fluctuation peak.

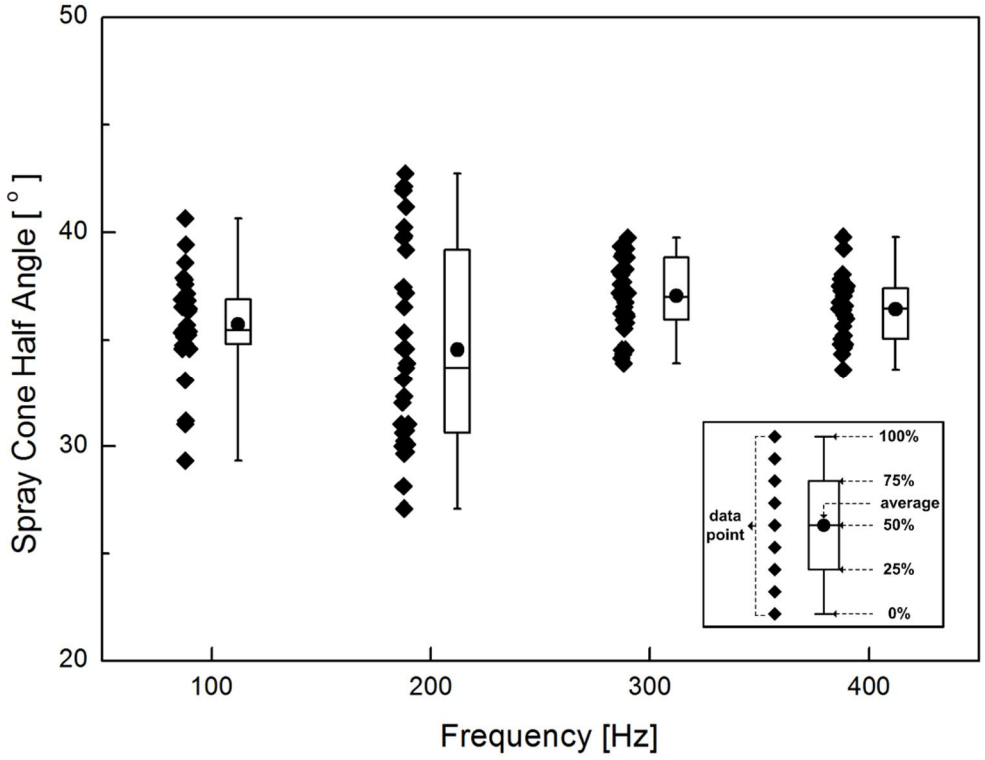

Fig. 3.19 Spray cone half angle characteristics of open type swirl injector with pulsation.

3.6 Effects of tangential entry number and manifold diameter

To determine the geometry parameter, which affects the fluctuation peak more effectively, injector parts to change the tangential entry number and manifold diameter were designed and manufactured. The same experiments and analyses were conducted as the swirl chamber length and diameter analyses. The explanation in section 3.2 with Eq. (3.1) and Eq. (3.2) is also valid for the tangential entry number variation, which is shown in Fig. 3.21(a), with a pulsation frequency range of 400–1,000 Hz. The geometric characteristic parameter A increases with decreasing tangential entry number, n_t, which results in the reduced amplitude of the liquid film thickness. However, at the pulsation frequency of 100–300 Hz, which is the nearby-peak region, this tendency is reversed. The amplitude peak is the largest at $n_t = 2$, and it is the smallest at $n_t = 4$. This result shows that Eq. (3.1) and Eq. (3.2) well express the phenomenon throughout most of the pulsation frequency regions except the peak, where another stronger physics due to the converging section—manifold and tangential entry—affects the amplitudes, resulting in an opposite tendency of the amplitudes. As the amplitudes in the nearby-peak region are much larger than the rest of the frequency range, the slope in Fig. 3.20(a) is greatly affected. The slope follows the tendency of the nearby-peak region, decreasing with an increasing tangential entry number, nt.

The manifold has been a rare issue in injector dynamics studies. However, it was found to be an influential parameter on the open-type swirl injector's dynamic characteristics through the experiment done in this study. Figure 3.20(b) shows the relation between the manifold pressure and the film thickness amplitude for the manifold variation. The maximum manifold pressure amplitude becomes smaller as the manifold diameter increases. This trend indicates that the enlarged manifold acts as a cavity installed in the feed system, absorbing the fluctuation. Therefore, even the average value of the liquid film thickness amplitude is at least $D_m = 56$mm, and the slope becomes the largest in Fig. 3.20(b). Figure 3.21(b) shows the liquid film thickness amplitude change caused by the manifold diameter variation throughout the pulsation frequencies. The

liquid film thickness amplitude decreases as the manifold diameter increases. As well, in the case of D_m = 56 mm, the fluctuation peak at 200 Hz is greatly diminished.

As the converging section in a closed-type swirl injector generates the fluctuation amplitude peak, the manifold and the tangential entry have dominant influence on the open-type swirl injector instead.[8, 9] The manifold plays a role as a cavity, and the tangential entry plays a role as a converging section. The fluctuation amplitude change due to the variation in geometry was much larger with the manifold diameter and tangential entry number than the swirl chamber length and diameter.

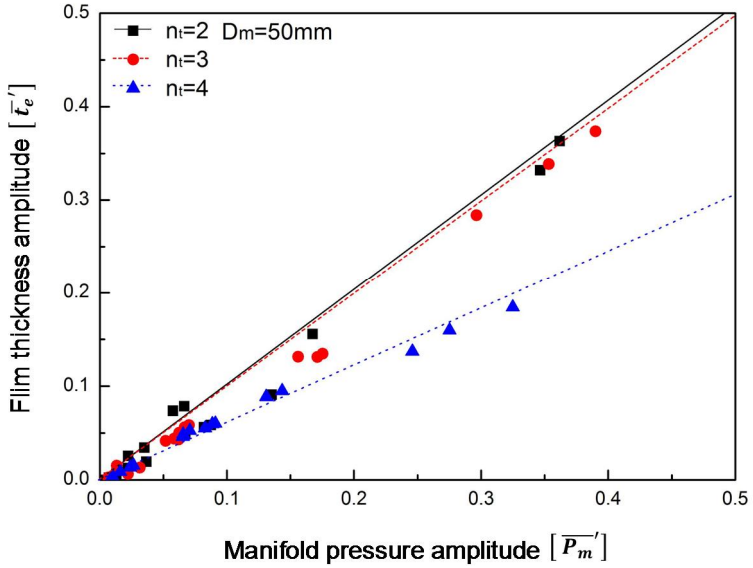

(a)

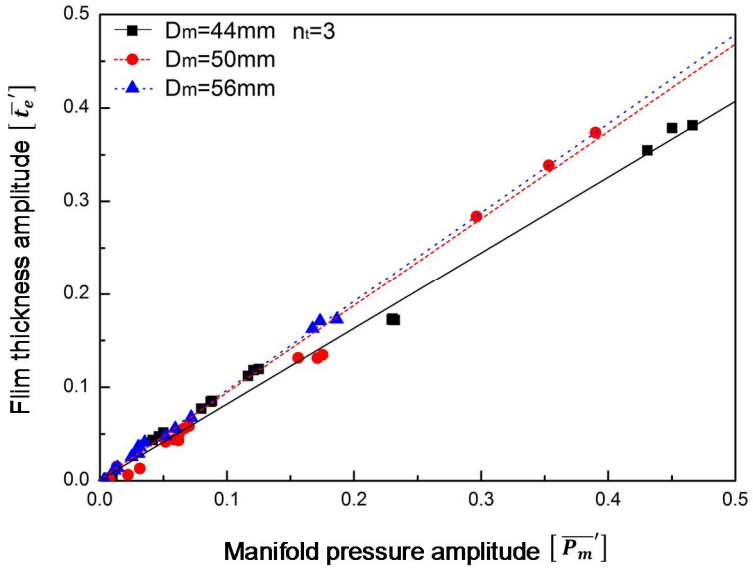

(b)

Fig. 3.20 Relation between manifold pressure and liquid film thickness amplitude for (a) tangential entry number variation and (b) manifold diameter variation.

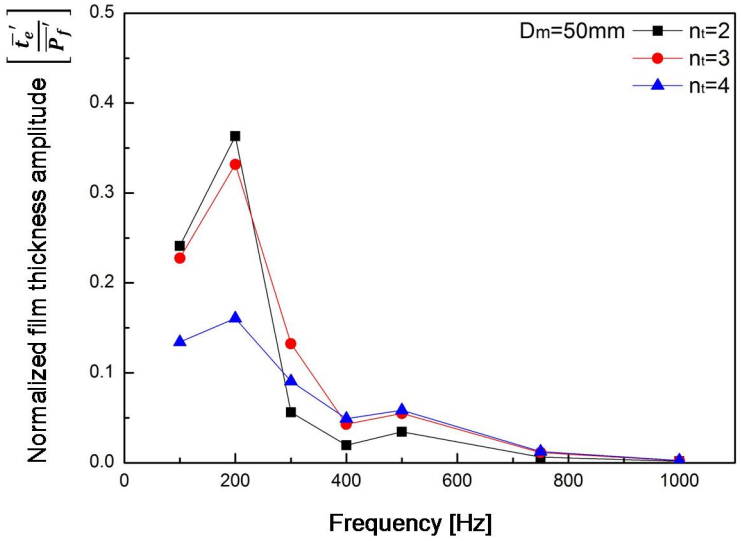

(a)

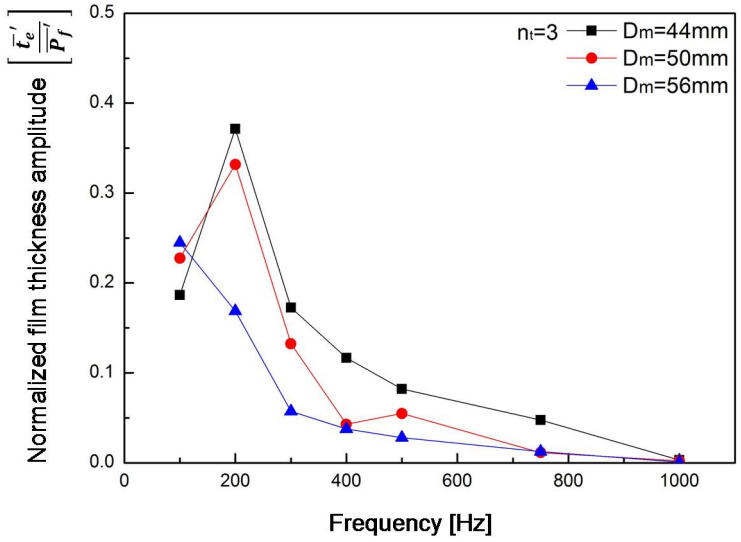

(b)

Fig. 3.21 Frequency–amplitude diagram of liquid film thickness amplitude for (a) tangential entry number variation and (b) manifold diameter variation.

3.7 Peak amplitude ratio change for each geometry parameter

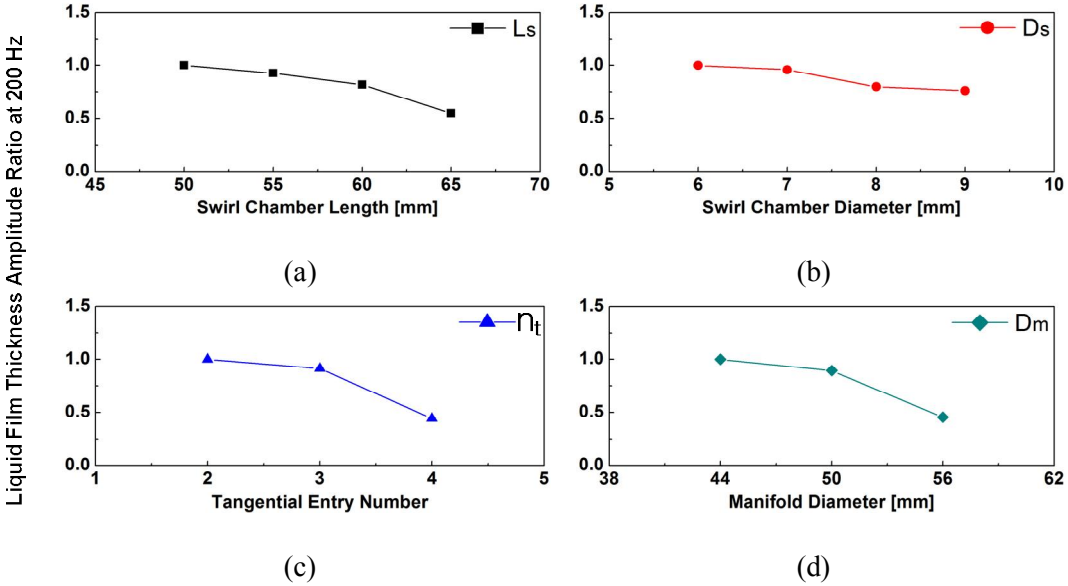

Fig. 3.22 Peak amplitude ratio at 200 Hz for each geometry parameter: (a) swirl chamber length; (b) swirl chamber diameter; (c) tangential entry number; (d) manifold diameter

The liquid film thickness amplitude at the fluctuation peak, 200 Hz was normalized with its largest value, as shown in Eq. (3.5), for each geometry parameter case, including L_s = 50 mm, D_s = 6 mm, n_t = 2, and D_m = 44 mm, respectively.

$$\textit{Film thickness amplitude ratio at 200 Hz} = \frac{\left[\frac{t_e'}{t_{e.avg}}\right]_{200hz}}{\left[\frac{t_e'}{t_{e.avg}}\right]_{200hz.\,max}} \tag{3.5}$$

Even though each geometry parameter's change cannot be compared directly, as the variation gap size for each parameter was selected to be reasonable, considering each parameter's size and characteristics, the effectiveness of each geometry parameter change

can be observed, as shown in Fig. 3.22. The fluctuation peak of the film thickness amplitude drops sharply with the case change of the manifold diameter and tangential entry number, and it drops relatively gradually with the case change of the swirl chamber length and diameter. This type of analysis can provide insight into injector designs when changing the injector's geometry for combustion instability suppression. However, every parameter in a liquid rocket design is multi-coupled with other parameters, so a modification to a certain parameter is not always possible. For example, it was found that a sufficient manifold size could be important to suppressing the disturbance from the feed line to the injector. However, as space is a very limited resource in liquid rockets, the manifold size cannot be expanded without limitations. The trade-offs are essential in designing liquid rocket engines, and this type of data should be obtained previously.

CHAPTER 4

DYNAMIC CHARACTERISTICS OF CLOSED-TYPE SWIRL INJECTOR

4.1 Closed-type swirl injector geometry

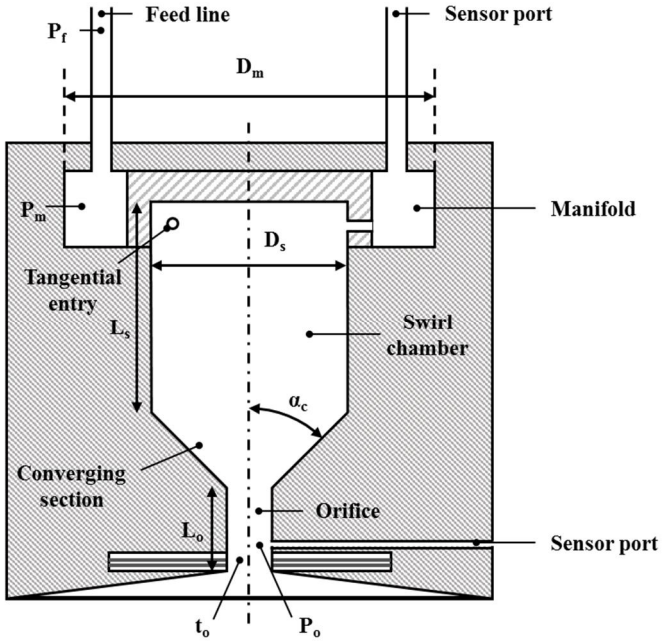

Fig. 4.1 Schematics of closed-type swirl injector.

Table 4.1 Closed-type swirl injector geometries.

D_m, mm	n_t	D_t, mm	L_s, mm	D_s, mm	L_o, mm	D_o, mm	α_c, °
50	3	1.4	30	20	15	6	45
50	3	1.4	30	25	15	6	45
50	3	1.4	30	30	15	6	45
50	3	1.4	60	30	15	6	45
50	3	1.4	30	30	15	6	90
50	3	1.4	30	30	15	6	22.5
50	3	1.4	30	30	30	6	45

Closed-type swirl injector with replaceable parts to change the geometry parameters was designed and manufactured. The sectional view schematic of a closed-type swirl injector is shown in Fig. 4.1. The injector parts were made of polycarbonate (PC) which is a non-conductive material to avoid interference with the titanium electrodes installed at the end of the orifice to measure the liquid film thickness. The geometry of the manifold part was designed to be same as the manifold of the open-type swirl injector for the comparison study. 4 major geometries were selected to be investigated through the experiments. Diameter of the swirl chamber D_s, length of the swirl chamber L_s, angle of the converging section α_c and length of the orifice L_o were the four selected geometry parameters. Pressures measured at the manifold and the orifice were denoted as P_m and P_o, respectively. And the liquid film thickness measure by the titanium electrodes at the end of the orifice was denoted as t_o. Table 4.1 shows the details of the geometry parameters selected for the experiment. The frequencies of the generated pressure oscillations in the feed line created by the hydrodynamic mechanical pulsator were 100–1,000 Hz. Fig. 4.2 shows the effect of different frequency intervals. Frequency interval was set to be 50 Hz in Fig. 4.2(a). To verify the interval was sufficient to describe the dynamic characteristics of the closed-type swirl injector, the near peak region was subdivided in to 10 Hz intervals. The results are shown in Fig. 4.2(b). The dynamic characteristics changes linearly and does not show any sudden peaks. Since additional frequencies require more time and resources, the adequate interval for closed-type swirl injector was decided as 50 Hz. The average manifold pressure when the pressure oscillations were produced was maintained at 4 bars which were the same in open-type swirl injector experiments.

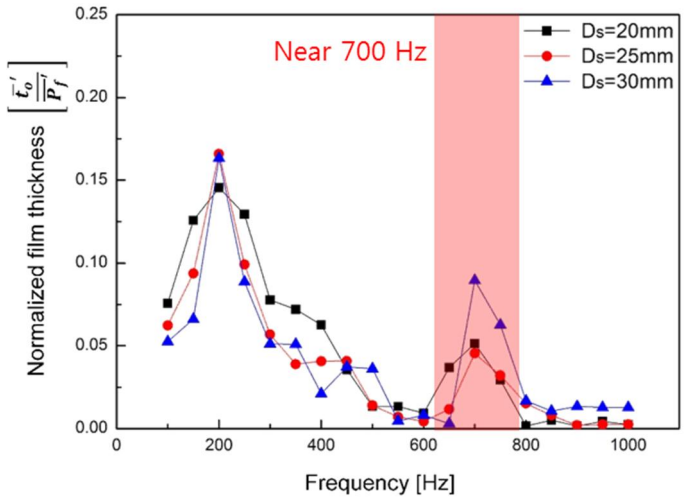

(a)

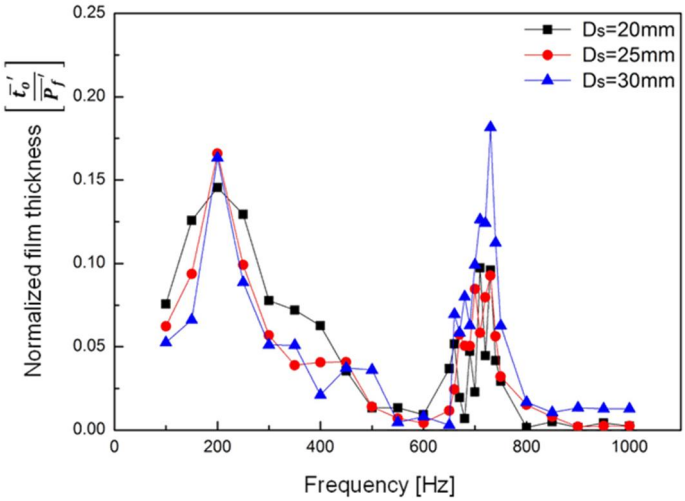

(b)

Fig. 4.2 Changes in dynamic characteristics with frequency intervals in closed type swirl injector.

4.2 Swirl chamber diameter variation

Swirl chamber diameter was investigated first, since it was reported to be the most influencing parameter for the dynamic characteristics.[9] Swirl chamber diameter influences both the injector geometry coefficient, A, and the injector closing extent, $\overline{R_s}$, which are major parameters in injector dynamics studies.

Figure 4.3 shows the dynamic characteristics of closed-type swirl injectors with varying swirl chamber diameters. Normalized manifold pressure amplitude is shown in Fig.4.3(a) and normalized liquid film thickness amplitude is shown in Fig.4.3(b). Each frequency points are averaged value and the maximum and minimum measured values of each frequency are marked. Normalized manifold pressure amplitude has a peak frequency at 200 Hz for all three swirl chamber diameter cases. Normalized manifold pressure amplitude decreases as swirl chamber diameter decreases, but the peak frequency remains constant at 200 Hz and does not show any secondary peak frequencies.

Normalized liquid film thickness show the same trend as the normalized manifold pressure amplitudes regarding the peak amplitudes, but there is a second peak frequency at 700 Hz. No additional peaks have been observed for open-type swirl injectors, so these 700 Hz peaks appear to be unique to the closed-type swirl chamber.[4]

These outcomes are consistent with prior research. Ismailov et al. calculated closed-type swirl injector response sensitivity to various pulsation frequencies, and showed multiple peak frequencies depending on the closed-type swirl injector geometry. The reflecting waves, caused by the converging section between the swirl chamber and orifice, are believed to trigger the resonance and establish the peak characteristics.[8, 9] Fu et al. modified Bazarov's equation for closed-type swirl injectors to apply to open-type swirl injectors and the open-type swirl injectors showed a smooth peak in the lower frequency region which decreased with increasing frequency.[17]

Consequently, more injector geometry parameters were selected and varied to find the tendencies and sensitivities of injector dynamic characteristics for each geometry parameter.

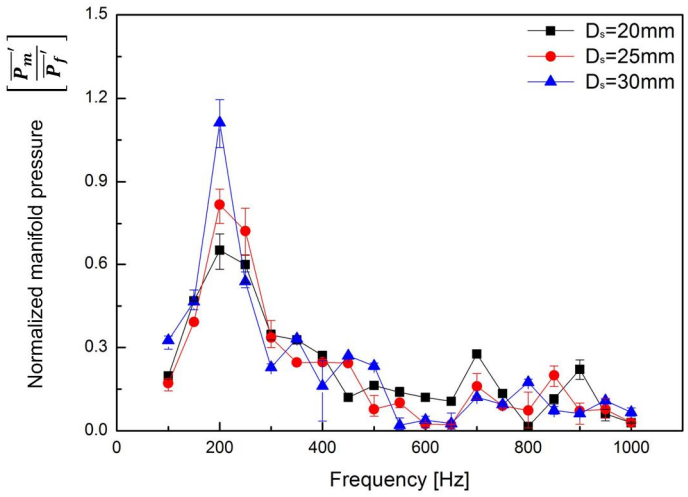

(a)

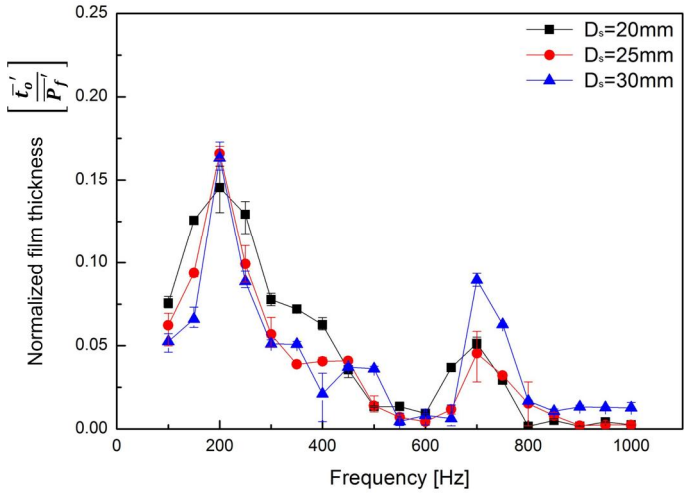

(b)

Fig. 4.3 Swirl chamber diameter variation effects: a) manifold pressure amplitude and b) liquid film thickness amplitude.

4.3 Swirl chamber length variation

Extending the swirl chamber length for closed-type swirl injectors is known to cause periodic decrease and increase in injector oscillation amplitude and increased phase angle.[2] This study used a long swirl chamber case with L_s = 60 mm, D_s = 30 mm. Figure 4.4(a) shows the normalized manifold pressure amplitude has discrete sequential peaks in the long swirl chamber case. Thus, manifold pressure is affected by the change in swirl chamber geometry, even though the manifold is located upstream of the swirl chamber. Figure 4.4(b) shows that the first peak (200 Hz) in normalized liquid film thickness amplitude decreases for the long swirl chamber, and a second peak appears at 450 Hz. Previous research on open-type swirl injectors has shown only a single peak frequency of liquid film thickness oscillation stimulated by the converging section.[4] Therefore, we assume the 200 Hz peak here is also produced by the manifold and tangential entries, in common with open-type swirl chambers, but the higher frequency peaks are unique to closed-type swirl injectors. The second peak frequency of normalized liquid film thickness amplitude moves from 700 Hz to 450 Hz as the swirl chamber length increases from 30 mm to 60 mm, and increases in amplitude slightly. This is also consistent with Ismailov's results. The resonant modes in the swirl chamber can be expressed as

$$\omega_0 = n\frac{\pi}{2L_v}\sqrt{C^2\frac{R_v^2-r_v^2}{2r_v^4}}, \tag{4.1}$$

where n = 1, 3, 5 ⋯. ACRM peaks calculated from equation (4.1) show that resonant frequencies decrease [9] and their amplitude increases with increasing as swirl chamber length, which is consistent with the current study.

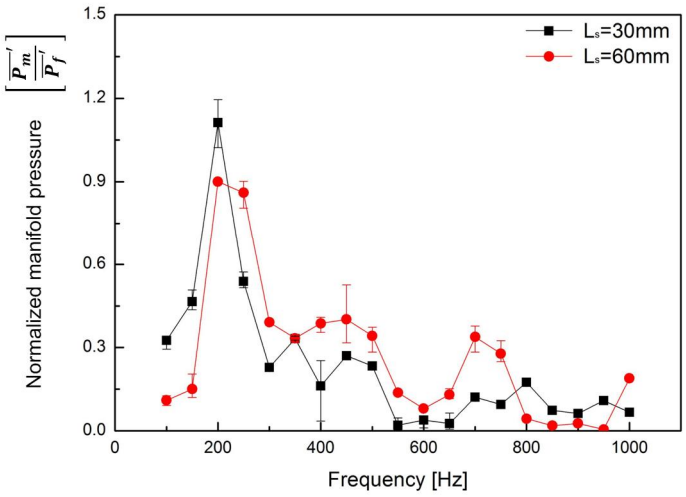

(a)

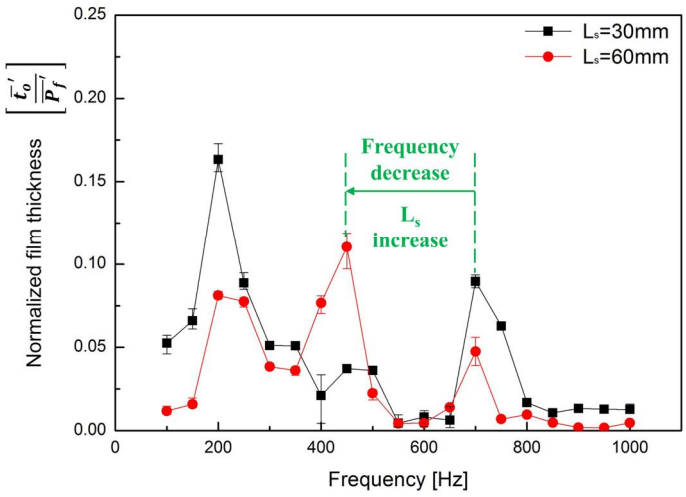

(b)

Fig. 4.4 Swirl chamber length variation effects: (a) manifold pressure amplitude and (b) liquid film thickness amplitude.

4.4 Converging angle variation

Three cases for the angle of the converging section between the swirl chamber and orifice, 22.5°, 45°, and 90°, were investigated. Swirl chamber diameter was fixed at 30 mm and Ls was fixed at 30 mm for each case. Figure 4.6 shows the normalized manifold pressure and normalized liquid film thickness. The first and second peak amplitudes of normalized liquid film thickness decrease as converging angle decreases. The second peak frequencies decreased significantly (from 950 Hz to 400 Hz), with only a modest decrease of the first peak frequency. Although the magnitude of frequency change is different, this tendency is also consistent with Ismailov. [9]

Figure 4.5 shows the geometry parameters in the swirl chamber, including swirl chamber length L_s, converging length L_c, and extended swirl chamber length $L_e = L_s + L_c$. The extended swirl chamber lengths for converging 90°, 45° and 22.5° converging angles were 30, 42, and 58.97 mm, respectively. For the 22.5° case, peak amplitude is particularly decreased. The reflection waves due to the converging section wall seem to be weakened since the orthogonal component decreases with decreasing angle. The detailed effects of converging angle should be investigated further using closed-type swirl injectors with same extended length but different converging angles.

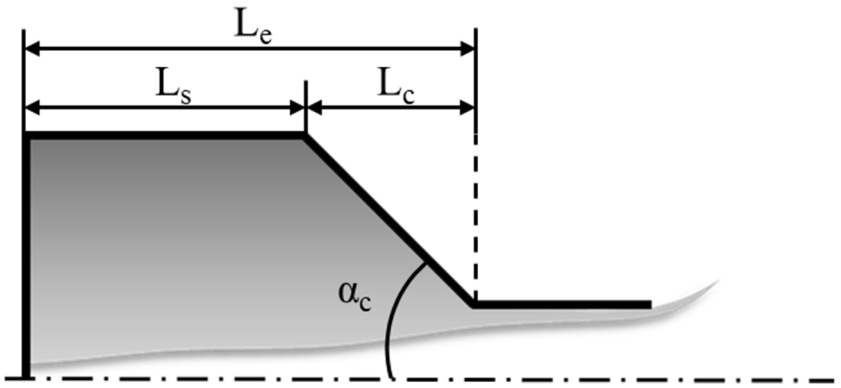

Fig. 4.5 Geometry parameters in the swirl chamber

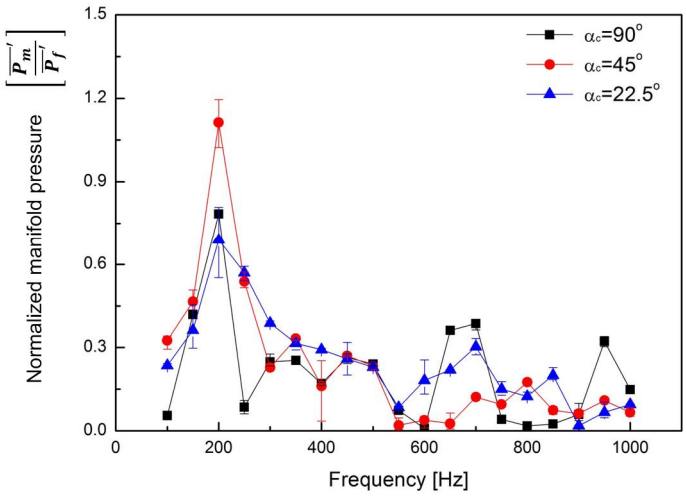

(a)

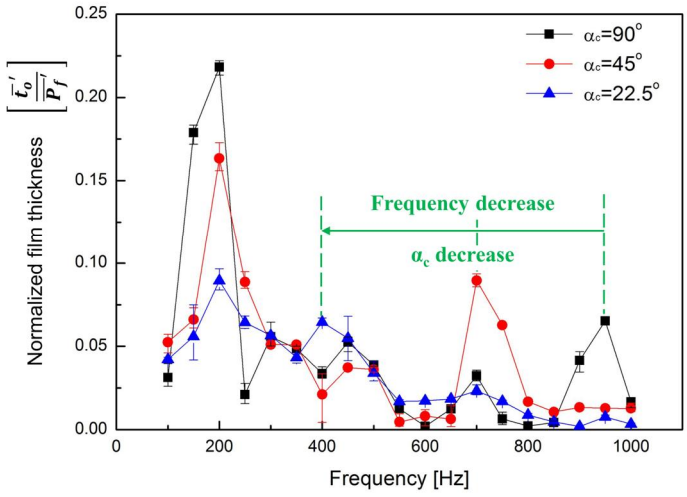

(b)

Fig. 4.6 Converging angle variation effects: a) manifold pressure amplitude and b) liquid film thickness amplitude

4.5 Orifice length variation

A long orifice (Lo = 30 mm, Ls = 30 mm, and Ds = 30 mm) was fabricated to investigate the orifice influence. Extending the orifice is expected to cause phase differences between the pressure drop and flow rate oscillations to increase, but not to have much effect on amplitudes.[2, 9] Fig. 4.7 shows good agreement between the experimental results and theory. The normalized amplitude of both manifold pressure and liquid film thickness show only small differences between the two orifice lengths, and only the normalized amplitudes at the 200 Hz peak decreased as the orifice length doubled. Although the 200 Hz peak is created by the manifold region and the 700 Hz peak by the closed swirl chamber, geometry changes in the orifice also affect the manifold pressure. Thus, a change in geometry can cause dynamic characteristic changes of other parts of the injector.

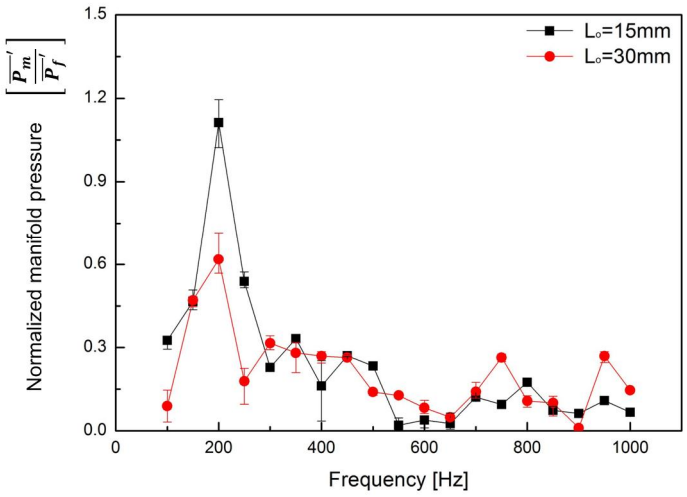

(a)

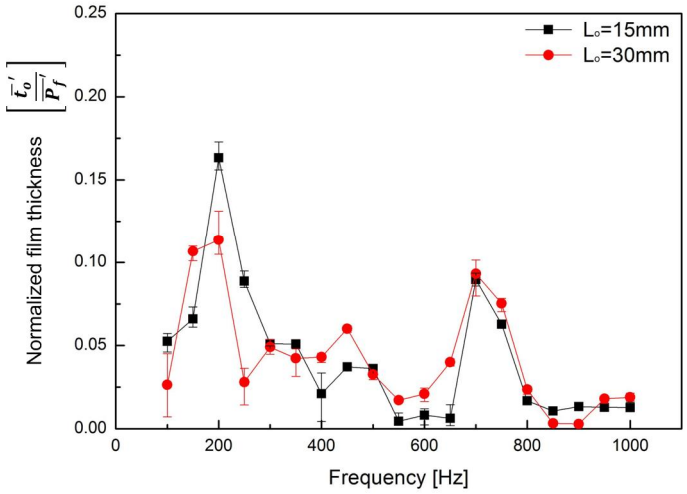

(b)

Fig. 4.7 Orifice length variation effects: a) manifold pressure amplitude and b) liquid film thickness amplitude.

4.6 Spray structures

Pulsated spray images were taken with the high speed camera to investigate the spray structure, as shown in Fig. 4.8 for 30 mm swirl chamber diameter. The spray images were taken in steady state and pulsated states at the frequency of the second peak generated by the closed-type swirl chamber, in this case 700 Hz. The time interval between each image is approximately 0.0004 s. Fig. 4.8(a) shows that the steady state produces smooth cone shaped spray. Unlike the large fluctuations which have been shown for open-type swirl injectors, only relatively small bumps occurred in the spray. However, Fig. 4.8(b) shows a small bump occurs every 0.0014 s for the 700 Hz case. The bumps develop as they travel downstream from the injector orifice. The bump marked as (1) travels downstream until it reaches the break up region. Bump (2) and subsequent bumps follow the same sequence. This visualization of the spray dynamics shows that the dynamic characteristics within the injector are coupled with spray structures outside the injector, and eventually influence the combustion process.

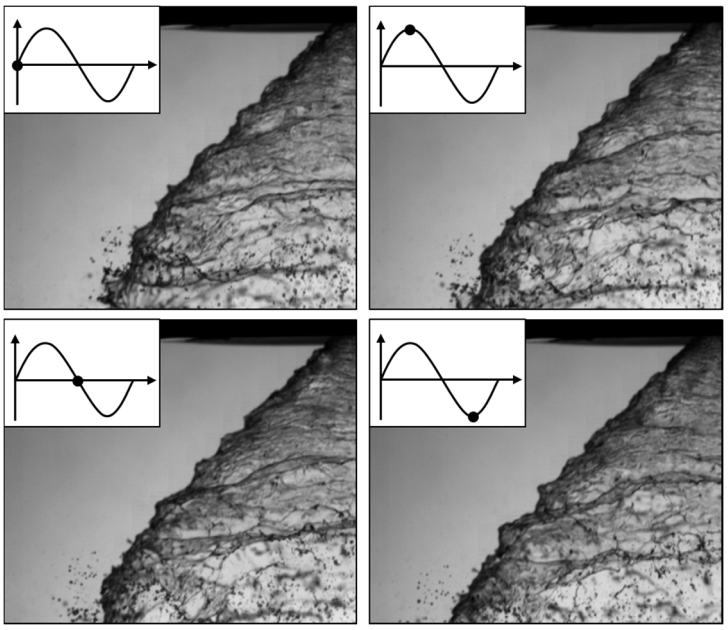

(a)

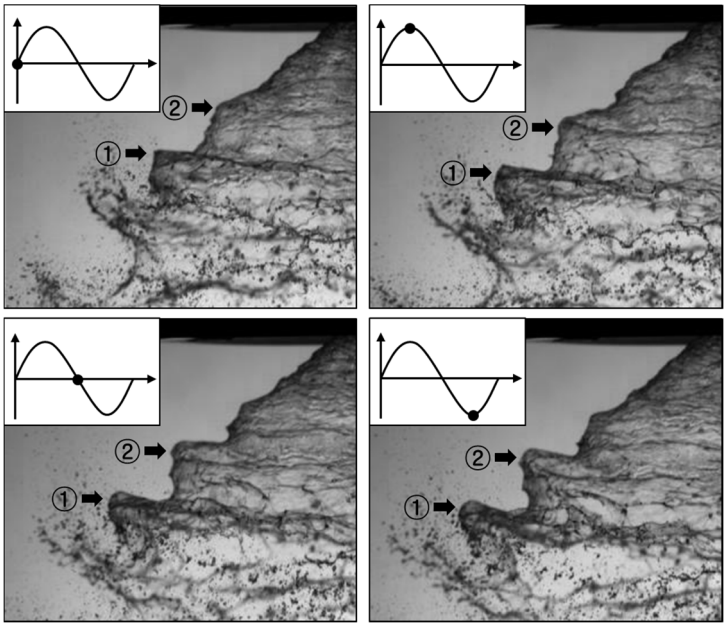

(b)

Fig. 4.8 Spray structure: a) 0 Hz and b) 700 Hz

4.7 Influence of swirl chamber length on the second peak frequency

Table 4.2 Geometry parameters for extended swirl chamber length variation cases.

Case	L_s, mm	L_c, mm	L_e, mm	α_c, °
(a)	30	0	30	90
(b)	30	12	42	45
(c)	30	28.97	58.97	22.5
(d)	60	12	72	45

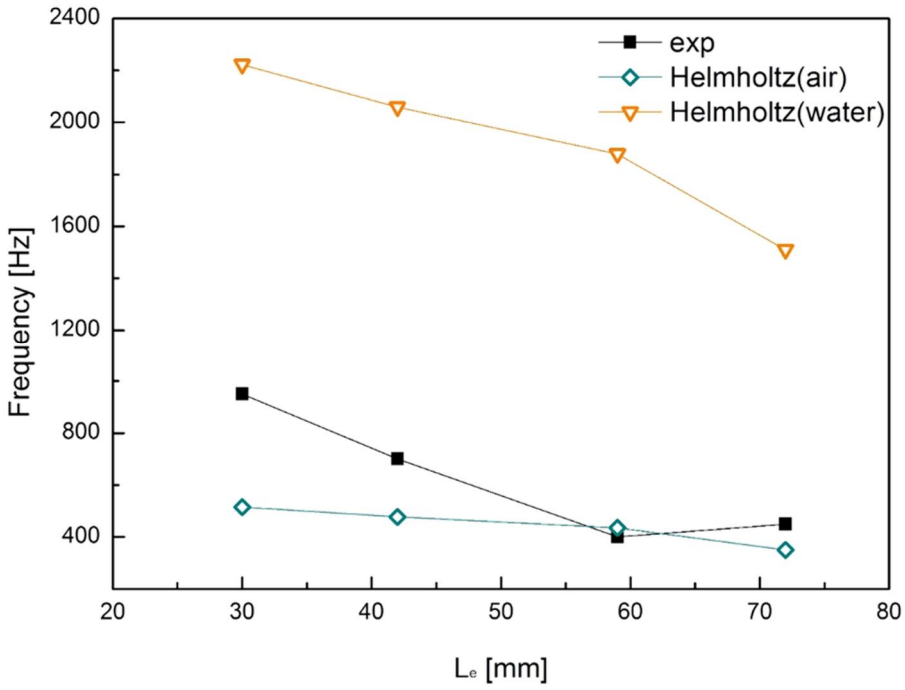

Fig. 4.9 Comparison with Helmholtz resonator frequencies

Table 4.1 shows the extended swirl chamber lengths investigated here. Since the peak frequencies decrease with increasing chamber length, the swirl chamber is working as a resonating chamber. The fluid filling the injector swirl chamber consists of two parts, the liquid film (water), and the air core. Therefore, Helmholtz resonant frequencies were calculated for both type of fluids assuming the swirl chamber to be a Helmholtz resonator, as shown in Fig. 4.9. Helmholtz resonant frequencies for the swirl chamber filled with only air and only water are shown separately. The calculated and experimental results have similar tendency to decrease with increasing L_e, but the values show some discrepancy since the Helmholtz resonant frequency assumes monotonous phase, which is not the actual state inside the swirl chamber. Bazarov's transfer function that models the actual state inside the swirl chamber more precisely were applied, [2]

$$\Pi_{\Phi} = \frac{Q'_c}{Q_c} \Big/ \frac{\Delta p'_{\Phi}}{\Delta p_{\Phi}} = \frac{\bar{R}_к^2}{a} \cdot \frac{\Pi_c \cdot \Pi_{к.cII} \cdot \Pi_т}{2\Pi_т(\Pi_{к.зII}+\Pi_{к.зIII})+1} \tag{4.2}$$

The transfer function comprises three transfer functions for tangential entry, swirl chamber, and orifice, which are the main three components of the swirl injector, [2]

$$\begin{cases} Re\Pi_т = 1/2\,(1+Sh_т^2)\,; \\ Im\Pi_т = -Sh_т/2(1+Sh_т^2)\,; \end{cases} \tag{4.3}$$

$$\begin{cases} Re\Pi_{к.зII} = K_{\Sigma II}\sum_{n=0}^{n=\infty}\Pi^n\, cos(2n\Phi_к)e^{-2\nu n\Phi_к/2\pi}\,; \\ Im\Pi_{к.зII} = -K_{\Sigma II}\sum_{n=0}^{n=\infty}\Pi^n\, sin(2n\Phi_к)e^{-2\nu_n\Phi_к/2\pi}\,; \end{cases} \tag{4.4}$$

$$\begin{cases} Re\Pi_{к.зIII} = \frac{\bar{R}_к-\sqrt{a}}{\bar{R}_к}\int_0^1 cos\, f(\bar{x})d\bar{x} \;\Big/\; (1-\frac{\bar{R}_к-\sqrt{a}}{\bar{R}_к}\bar{x})^3\,; \\ Im\Pi_{к.зIII} = \frac{\bar{R}_к-\sqrt{a}}{\bar{R}_к}\int_0^1 sin\, f(\bar{x})dx \;\Big/\; (1-\frac{\bar{R}_к-\sqrt{a}}{\bar{R}_к}\bar{x})^3\,; \end{cases} \tag{4.5}$$

$$\begin{cases} Re\Pi_{к.cII} = K_{\Sigma II}\sum_{n=0}^{n=\infty}\Pi^n\, cos[(2n+1)\Phi_к]e^{-\nu(2n+1)\Phi_к/2\pi}\,; \\ Im\Pi_{к.cII} = -K_{\Sigma II}\sum_{n=0}^{n=\infty}\Pi^n\, sin[(2n+1)\Phi_к]e^{-\nu(2n+1)\Phi_к/2\pi}\,; \end{cases} \tag{4.6}$$

$$\begin{cases} |\Pi_c| = (1-\Pi) = 2\sqrt{\varphi}/\sqrt{\bar{R}_к^2 - a}\ ; \\ arg\Pi_c = \psi_c = -\omega\, L_c/v_c\ ; \end{cases} \tag{4.7}$$

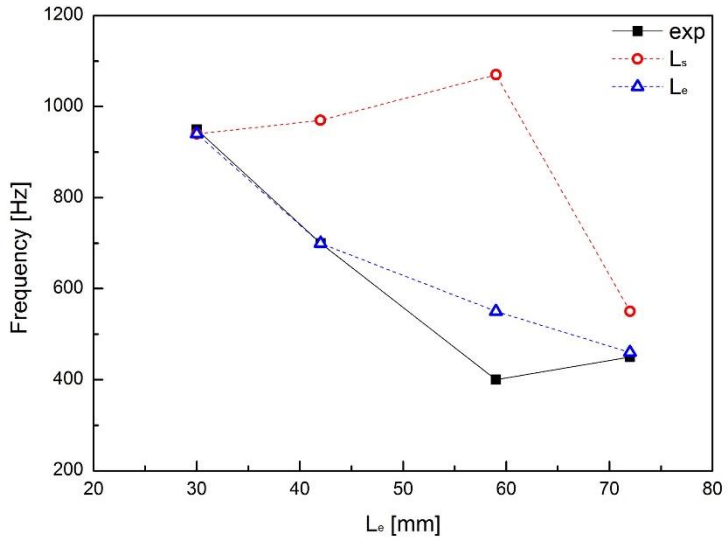

Fig. 4.10 Peak frequency change with swirl chamber length variation.

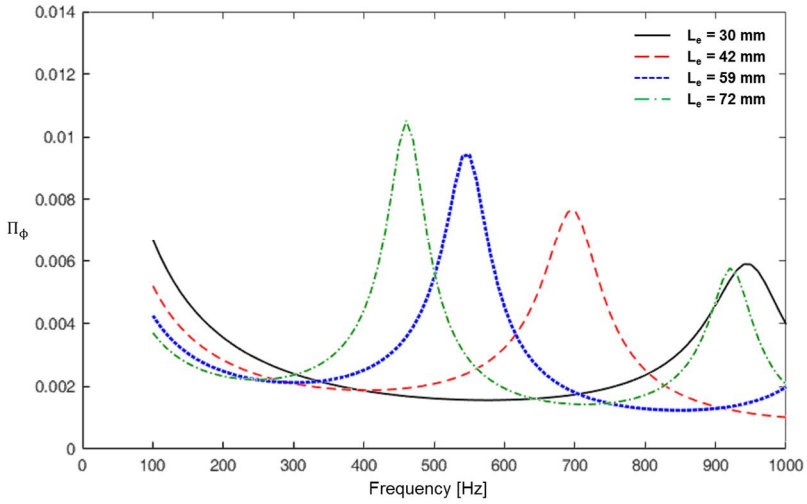

Fig. 4.11 Transfer function for extended swirl chamber lengths.

Dynamic characteristic peaks for each swirl injector geometry case were obtained from these transfer functions as shown in Fig. 4.10. However, definition of 'swirl chamber length' were not given in schematic form. Accordingly, both swirl chamber length of L_s and L_e were applied independently. Since there are no parameters representing the converging angle in the transfer function, only L_s could describe variations of the injectors. Thus, the calculated result shows large deviation from the experimental results.

The current form of transfer function is not capable of reflecting changes in the converging angle. As stated previously, decreasing the converging angle affects the dynamic characteristics of the swirl injector as if the length of swirl chamber was extended, because the length of converging section, L_c, extends with decreasing converging angle. Therefore, the sum of swirl chamber length, L_s and converging section length, L_c were defined as the extended swirl chamber length, L_e. The calculation results based on the transfer function are shown in Fig. 4.11.[28]

Since the transfer function only considers three parts the swirl injector (tangential entry, swirl chamber, and orifice) dynamic characteristics that arise from upstream of the injector are excluded. Therefore, the first peak frequency of the transfer function is matched with the second peak frequency of the experimental results. The recalculated results are shown in Fig. 4.10, denoted as L_e. The peak frequencies of the dynamic characteristics for the transfer function with L_e match well with the experimentally measured peak frequencies.

The accuracy of the conventional injector transfer function was superior using swirl chamber length of L_e than L_s. Fig. 4.12 shows that the disturbances that arise from the different sources in a wide range of frequencies fade out for most of the frequency range, but frequencies that coincide with the characteristic length of the injector (L_e) resonate within the injector structure. This resonance can obstruct stable propellant delivery,

causing combustion instability. Thus, the transfer function can predict the peak frequency change caused by varying the swirl chamber length, thereby allowing designers to avoid combustion instability in liquid rocket engines.

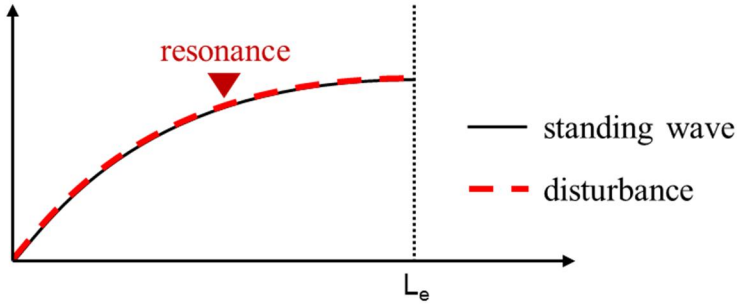

(a)

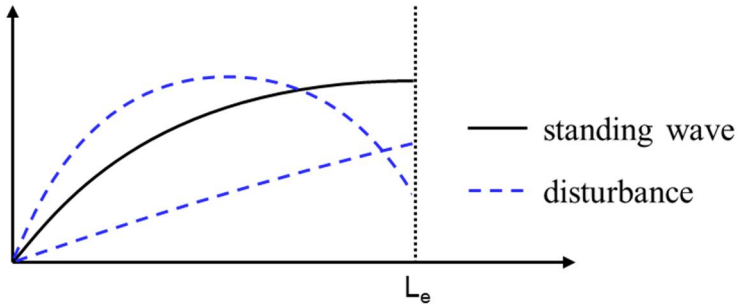

(b)

Fig. 4.12 Resonance in the injector swirl chamber: a) resonance and b) non-resonance.

CHAPTER 5

CONCLUSION

The dynamic characteristics of open and closed-type swirl injectors with varying geometries were investigated. A hydrodynamic mechanical pulsator generated sinusoidal pressure pulsations in the feed line. Pressure in the feed line were measured to observe the pulsation characteristics of the hydrodynamic mechanical pulsator. The pulsator's dynamic characteristic showed relatively uniform over the experimental frequency range. The pressure in the manifold and at the exit of the swirl chamber, as well as the liquid film thickness at the exit of the swirl chamber, were measured to investigate the open-type and closed-type swirl injectors' dynamic responses to the given frequencies of the pressure pulsations by the hydrodynamic mechanical pulsator.

At first, the diameter and length of the swirl chamber's influences on the open-type swirl injector's dynamic characteristics were investigated. The amplitude of the liquid film thickness at the exit of the swirl chamber was proportional to the amplitude of the pressure in the manifold, and the average slope of each case decreased as the swirl chamber diameter and length were increased. Furthermore, the amplitude of the liquid film thickness at the exit of the swirl chamber had a maximum peak at a pulsation frequency of 200 Hz for all swirl chamber lengths and diameters. Theoretically, the dynamic characteristics of open-type swirl injector should smoothly and constantly as the frequency increases. This peak was found out to be caused by the interference between the incident wave from the feed line and reflected wave from the manifold. The fluctuation peak amplitude decreased with the increasing swirl chamber length and diameter, but the differences between each geometry variation were not large. For this reason, two more geometry parameters of an open-type swirl injector were selected for further experimental study. The largest amplitude point at the pulsation frequency of 200 Hz was also observed through spray images. The spray cone half angle was measured with the spray image, and the average spray cone half angle was almost the same at 100,

200, 300, and 400 Hz. However, the instantaneous spray cone half angle changed within the largest range at a pulsation frequency of 200 Hz, which is the observed largest amplitude point with the liquid film thickness measurement results. The manifold diameter and tangential entry number were the two newly selected geometry parameters, and the same experiments were conducted and analyzed. The amplitude of the liquid film thickness at the exit of the swirl chamber was also proportional to the amplitude of the pressure in the manifold, and the average slope decreased as the tangential entry number increased and manifold diameter decreased. The amplitude of the liquid film thickness at the exit of the swirl chamber had constant decreasing characteristics as the frequency increase, but the liquid film thickness amplitudes drastically decreased when the tangential entry number was 4 and the manifold diameter was 56 mm. The manifold diameter and tangential entry number more effectively impacted the dynamic characteristics of the open-type swirl injector than the length and diameter of the swirl chamber.

Closed-type swirl injector dynamic characteristics were investigated by analyzing the normalized liquid film thickness amplitude for different injector geometries also. In contrast to previously studied open-type swirl injectors, the normalized liquid film thickness amplitude of the closed-type swirl injector showed two peak frequencies for every geometry case. The first peak frequency, resulting from the converging section between the manifold and tangential entries, also existed in the closed-type swirl injector. However, a second peak frequencies appears only in the closed-type swirl injector, resulting from the converging section between the swirl chamber and orifice. The first peak frequency occurs at 200 Hz, which is the same as the open-type swirl injector. The second peak frequency occurs at 700 Hz for all swirl chamber diameters, although the amplitude of normalized liquid film thickness increased as the swirl chamber diameter increased. The second peak frequency of the normalized liquid film thickness moved from 700 Hz to 450 Hz with a slight amplitude increase as swirl chamber length was extended from 30 mm to 60 mm. The amplitude of the normalized liquid film thickness peak at 200 Hz decreased as the converging angle decreased from 90° to 22.5°, with no

significant change in peak frequency. However, the second peak frequency reduced from 950 Hz to 400 Hz over the same angle change. There was no significant change in amplitude or peak frequency for normalized liquid film thickness as orifice length extended from 15 mm to 30 mm. The experimentally measured swirl chamber peak frequencies for different swirl chamber lengths were compared with the conventional injector transfer function. Superior accuracy was derived using the extended swirl chamber length, L_e, in the transfer function than the actual swirl chamber length, L_s.

Experimental results showing each injector geometry parameter's effect on the dynamic characteristics in frequency domain were obtained. Sensitivity and tendency of the geometry parameters were shown. As a result, a way to suppress combustion instability with injector's dynamic characteristics by manipulating the peak frequency were suggested.

REFERENCES

[1] I. Keller, "Liquid rocket engine combustion stabilization devices," *NASA SP-8113,* 1974.

[2] V. Bazarov, "Liquid Injector Dynamics," *Mashinostroenie,* 1979.

[3] V. G. Bazarov and V. Yang, "Liquid-Propellant Rocket Engine Injector Dynamics," *Journal of Propulsion and Power,* vol. 14, no. 5, pp. 797-806, 1998.

[4] Y. Chung, H. Kim, S. Jeong, and Y. Yoon, "Dynamic Characteristics of Open-Type Swirl Injector with Varying Geometry," *Journal of Propulsion and Power,* vol. 32, no. 3, pp. 583-591, 2016.

[5] T. Khil, Y. Chung, V. G. Bazarov, and Y. Yoon, "Dynamic Characteristics of Simplex Swirl Injector in Low Frequency Range," *Journal of Propulsion and Power,* vol. 28, no. 2, pp. 323-333, 2012.

[6] F. E. C. Culick and V. Yang, "Overview of combustion instabilities in liquid-propellant rocket engine," *AIAA Progresses in Astronautics and Aeronautics,* vol. 169, pp. 3-38, 1995.

[7] V. Bazarov, "Self-Pulsations in Coaxial Injectors with Central Swirl Liquid Stage," *31st AIAA/ASME/SAE/ASEE Joint Propulsion Conference and Exhibit,* 1995.

[8] M. Ismailov and S. D. Heister, "Dynamic Response of Rocket Swirl Injectors, Part I: Wave Reflection and Resonance," *Journal of Propulsion and Power,* vol. 27, no. 2, pp. 402-411, 2011.

[9] M. Ismailov and S. D. Heister, "Dynamic Response of Rocket Swirl Injectors, Part II: Nonlinear Dynamic Response," *Journal of Propulsion and Power,* vol. 27, no. 2, pp. 412-421, 2011.

[10] B. Ahn, M. Ismailov, and S. Heister, "Experimental Study on Swirl Injector Dynamic Response Using a Hydromechanical Pulsator," *Journal of Propulsion and Power,* vol. 28, no. 3, pp. 585-595, 2012.

[11] M. Wilson, D. Lineberry, and M. Moser, "Experimental Pulsator Characterization

for Liquid Injector Research," *45th AIAA/ASME/SAE/ASEE Joint Propulsion Conference and Exhibit,* 2009.

[12] T. Khil, S. Kim, S. Cho, and Y. Yoon, "Quantification of the Transient Mass FlowRate in a Simplex Swirl Injector," *Measurement Science and Technology,* vol. 20, no. 7, p. 075405, 2009.

[13] L.-J. Yang and Q.-F. Fu, "Theoretical Investigation on the Dynamics of a Gas-Liquid Coaxial Swirl Injector," *Journal of Propulsion and Power,* vol. 27, no. 1, pp. 144-150, 2011.

[14] Y. Chung, T. Khil, J. Yoon, and Y. Yoon, "Experimental Study on Simplex Swirl Injector Dynamics with varying Geometry," *International Journal of Aeronautical and Space Science,* vol. 12, no. 1, pp. 57-62, 2011.

[15] Q.-F. Fu, L. Yang, Y.-Y. Qu, and B. Gu, "Geometrical Effects on the Fluid Dynamics of an Open-End Swirl Injector," *Journal of Propulsion and Power,* vol. 27, no. 5, pp. 929-936, 2011.

[16] Q.-f. Fu, L.-j. Yang, and Y.-y. Qu, "Measurement of annular liquid film thickness in an open-end swirl injector," *Aerospace Science and Technology,* vol. 15, no. 2, pp. 117-124, 2011.

[17] Q.-F. Fu, L.-J. Yang, and X.-D. Wang, "Theoretical and Experimental Study of the Dynamics of a Liquid Swirl Injector," *Journal of Propulsion and Power,* vol. 26, no. 1, pp. 94-101, 2010.

[18] D. Harrje and F. Reardon, "Liquid propellant rocket combustion instability," *NASA SP-194,* 1972.

[19] J. Koo, "Rocket engineering," (in Korean), 2008.

[20] V. Bazarov, E. Lee, D. Lineberry, B. Swanner, and F. J. R., "Pulsator Designs for Liquid Rocket Injector Research," *43rd AIAA/ASME/SAE/ASEE Joint Propulsion Conference and Exhibit,* 2007.

[21] M. Suyari and A. H. Lefebvre, "Film thickness measurements in a simplex swirl atomizer," *Journal of Propulsion and Power,* vol. 2, no. 6, pp. 528-533, 1986.

[22] S. Kim, "Master thesis."

[23] S. Moon, E. Abo-Serie, and C. Bae, "Liquid film thickness inside the high pressure swirl injectors: Real scale measurement and evaluation of analytical equations," *Experimental Thermal and Fluid Science,* vol. 34, no. 2, pp. 113-121, 2010.

[24] S. Kim, T. Khil, D. Kim, and Y. Yoon, "Effect of geometric parameters on the liquid film thickness and air core formation in a swirl injector," *Measurement Science and Technology,* vol. 20, no. 1, p. 015403, 2009.

[25] N. Rizk and A. Lefebvre, "Internal flow characteristics of simplex swirl atomizers," *Journal of Propulsion and Power,* vol. 1, no. 3, pp. 193-199, 1985.

[26] A. H. Lefebvre, "Atomization and sprays," 1989.

[27] T. Marchione, C. Allouis, A. Amoresano, and F. Beretta, "Experimental Investigation of a Pressure Swirl Atomizer Spray," *Journal of Propulsion and Power,* vol. 23, no. 5, pp. 1096-1101, 2007.

[28] K. Ahn and H.-S. Choi, "Combustion Dynamics of Swirl Coaxial Injectors in Fuel-Rich Combustion," *Journal of Propulsion and Power,* vol. 28, no. 6, pp. 1359-1367, 2012.

초 록

액체로켓엔진에 있어서 연료 분사기는 핵심적인 역할을 하고 있는 부품으로서, 엔진의 개발 과정에서 연소불안정이 발생하였을 때 이를 저감하기 위하여 가장 먼저 변경하는 부품 중 하나이다. 그러나 이러한 과정은 현재까지 특정한 기준 없이 현장에서의 경험과 반복 시험을 통하여 진행되고 있는 실정으로 인젝터의 동특성 파악을 통한 기준점의 제시가 시급한 상황이다. Open-type과 Closed-type 스월 인젝터는 각각의 장단점에 따라 액체로켓엔진에 채택되어 널리 사용되고 있는데, 본 연구는 이러한 두 타잎의 스월 인젝터의 동적 특성을 실험적으로 분석한 연구로서 스월 인젝터에 존재하는 각각의 형상 인자들이 인젝터의 동특성에 미치는 영향의 경향성과 민감도를 파악하고자 하였다. 이를 위하여 액체로켓엔진의 운용 시 내부에서 발생될 수 있는 다양한 주파수의 섭동들을 모사하기 위하여 기계식 펄세이터가 설계 및 제작되었으며, 인젝터 출구에서의 액막 두께를 측정할 수 있는 장치도 제작되었다. 인젝터로 공급되는 유체의 공급 라인에서 측정되는 압력 신호를 입력으로, 인젝터의 출구에서 측정되는 액막 두께의 신호를 출력으로 선정하여 인젝터의 동특성을 분석하였다. 인젝터의 스월 챔버 길이, 지름과 스월챔버-오리피스 연결부의 각도, 오리피스의 길이, 매니폴드의 지름, 접선 방향 유입구의 개수 등의 형상 인자들이 각각 시험되었으며, 인젝터의 동특성에 지배적인 영향을 끼치는 형상 인자들이 밝혀졌다. 이러한 실험결과들은 향후 액체로켓엔진의 설계 제작 시 발생하는 연소 불안정을 저감하기 위한 인젝터 구조 변경의 방향성을 제시해 줄 수 있을 것으로 예상된다.

중심어: Open-type & Closed-type 스월 인젝터, 스월 챔버, 오리피스, 펄세이터, 동특성, 액막 두께

학 번: 2010-30967